

Status of MSSM Higgs Sector using Global Analysis and Direct Search Bounds, and Future Prospects at the HL-LHC

Biplob Bhattacharjee^{a1}, Amit Chakraborty^{b2}, and Arghya Choudhury^{c3}

^a Centre for High Energy Physics,
Indian Institute of Science, Bangalore 560012, India

^b Department of Theoretical Physics, Tata Institute of Fundamental Research,
1, Homi Bhabha Road, Mumbai 400005, India

^c Regional Centre for Accelerator-based Particle Physics,
Harish-Chandra Research Institute, Jhansi, Allahabad - 211019, India

Abstract

In this paper, we search for the regions of the phenomenological minimal supersymmetric standard model (pMSSM) parameter space where one can expect to have moderate Higgs mixing angle (α) with relatively light (up to 600 GeV) additional Higgses after satisfying the current LHC data. We perform a global fit analysis using most updated data (till December 2014) from the LHC and Tevatron experiments. The constraints coming from the precision measurements of the rare b-decays $B_s \rightarrow \mu^+ \mu^-$ and $b \rightarrow s \gamma$ are also considered. We find that low M_A ($\lesssim 350$) and high $\tan \beta$ ($\gtrsim 25$) regions are disfavored by the combined effect of the global analysis and flavour data. However, regions with Higgs mixing angle $\alpha \sim 0.1 - 0.8$ are still allowed by the current data. We then study the existing direct search bounds on the heavy scalar/pseudoscalar (H/A) and charged Higgs boson (H^\pm) masses and branchings at the LHC. It has been found that regions with low to moderate values of $\tan \beta$ with light additional Higgses (mass ≤ 600 GeV) are unconstrained by the data, while the regions with $\tan \beta > 20$ are excluded considering the direct search bounds by the LHC-8 data. The possibility to probe the region with $\tan \beta \leq 20$ at the high luminosity run of LHC are also discussed, giving special attention to the $H \rightarrow hh$, $H/A \rightarrow t\bar{t}$ and $H/A \rightarrow \tau^+ \tau^-$ decay modes.

¹biplob@cts.iisc.ernet.in

²amit@theory.tifr.res.in

³arghyachoudhury@hri.res.in

Contents

1	Introduction	3
2	Global analysis and available pMSSM parameter space	5
2.1	Experimental inputs and Global fit analysis	5
2.2	Available MSSM parameter space	10
3	Bounds on MSSM heavy Higgses from direct searches	16
3.1	Neutral Higgs boson searches	16
3.1.1	Search for H with $\gamma\gamma$ final states	16
3.1.2	Search for H with WW final states	17
3.1.3	Search for H with hh ($b\bar{b}b\bar{b}$ and $b\bar{b}\gamma\gamma$) final states	18
3.1.4	Search for H/A with $\tau^+\tau^-$ final states	20
3.1.5	Search for A with Zh final states	21
3.2	Charged Higgs boson searches	23
3.2.1	Search for H^\pm with $\tau\nu$ and $c\bar{s}$ final states	23
3.2.2	Search for H^\pm with $t\bar{b}$ final states	24
4	SUSY Higgs : Future limits	25
4.1	Heavy Higgs search	25
4.1.1	Search for H with 4ℓ final states	25
4.1.2	Search for pseudoscalar A with $\ell^+\ell^-b\bar{b}$ final states	26
4.1.3	Search for H with di-higgs ($H \rightarrow hh \rightarrow b\bar{b}\gamma\gamma$) final states	27
4.1.4	Search for H/A with $t\bar{t}$ final state	29
4.1.5	Search for H/A with $\tau^+\tau^-$ final states	32
5	Conclusion	35

1 Introduction

The ATLAS and CMS collaborations have now confirmed the discovery of a charge neutral spin-0 particle with mass close to 125 GeV using the 7+8 TeV data at the LHC [1, 2]. The CDF and $D\bar{0}$ collaborations at the Tevatron have also reported the evidence of a SM-like Higgs boson with mass around 125 GeV [3] with Higgs boson decaying to $b\bar{b}$. Measurement of its various couplings with the Standard Model (SM) particles so far seems to be consistent with the predictions of the SM Higgs boson. The primary goal of the run-II of the LHC with increased center-of-mass energy and integrated luminosity would be the more detailed study of various properties of the observed Higgs boson. The production modes of the observed Higgs boson that are analyzed at the LHC are the gluon-gluon fusion (ggF), vector boson fusion (VBF), associated production with a W or Z bosons, and associated production with a top-antitop pair, while the decay modes of the Higgs boson that are studied by the ATLAS and CMS collaborations¹ are $\gamma\gamma$ [6, 7], WW [8, 9], ZZ [10, 11], $b\bar{b}$ [12, 13] and $\tau^+\tau^-$ [14, 15]. Note that, the di-photon and ZZ modes have been used to precisely measure the mass of the observed Higgs boson [16, 17]. Even though various coupling measurements at the LHC have already ruled out large deviations from the SM expectations, still the presence of uncertainties in coupling measurements do not rule out the possibility of having non-standard couplings of the observed Higgs boson. In fact, any small but statistically significant deviation from the SM expectations can be thought of as the first indication of new physics.

Supersymmetry (SUSY) [18–20] has been one of the most popular extensions of the SM, however a SUSY signature is yet to be observed at the LHC. Non-observation of sparticles at the LHC have placed severe constraints on various superparticle masses and couplings [21, 22]. The Higgs sector of the CP conserving minimal supersymmetric standard model (MSSM) contains two CP-even neutral Higgs bosons h and H , one CP-odd neutral Higgs boson A , and two charged Higgs bosons H^\pm . One can identify the observed 125 GeV Higgs boson with the lightest MSSM Higgs boson h . At the tree level, the Higgs sector of MSSM is described by two parameters: pseudoscalar mass M_A and $\tan\beta$, where $\tan\beta$ is the ratio of the vacuum expectation values (vevs) of the two Higgs doublets H_u and H_d . The mixing angle α between the neutral components of the two Higgs doublets can be determined in terms of M_A and $\tan\beta$ at the tree level. However, radiative corrections to the Higgs boson mass matrix involving various SUSY parameters can modify the tree level value of α significantly. Moreover, the couplings of the lightest Higgs boson h with the SM particles depend on α and β , and thus a global fit analysis considering various Higgs coupling measurements at the LHC and Tevatron experiments can, in principle, constrain the MSSM parameter space.

Soon after the discovery of the 125 GeV Higgs boson, several analyses have been performed, for example, in the context of MSSM [23–38], general 2-Higgs doublet models [39–45], next-to minimal supersymmetric standard model (NMSSM) [46], effective theory framework [47–53]. However, in

¹Recently, search for the SM-like Higgs boson decaying to $\mu^+\mu^-$ and e^+e^- are also performed by both the ATLAS and CMS collaborations with 7+8 TeV LHC data [4, 5].

the last few months, both the ATLAS and CMS collaborations have updated some of their analyses on Higgs signal strength measurements. For example, ATLAS has updated their results for Higgs decaying to $\gamma\gamma$ [6], WW [8], ZZ [10], $b\bar{b}$ [12] channels, while CMS has published their new result for Higgs decaying to $\gamma\gamma$ [7]. In most of their analyses, the measure of uncertainty associated to various Higgs couplings have been now reduced by a sizable amount. A global analysis with the most updated (up to December 2014) results on various Higgs coupling measurements at the LHC and Tevatron would be extremely useful to probe the MSSM parameter space.

In order to probe the Higgs sector of the MSSM, the discovery or exclusion of additional Higgs boson is extremely crucial at the LHC. In addition to several extensive studies of the sparticles of the MSSM, both the ATLAS and CMS collaborations have also performed dedicated searches of these additional Higgses in various possible final state signatures at the LHC. Searches for the heavy Higgses (both H and A) are performed at the LHC when they are produced via the gluon-gluon fusion and b -associated production processes with their decay to a pair of τ s [54, 55]. The ATLAS and CMS collaborations have also searched for the heavy resonances with the following decay modes: $H \rightarrow \gamma\gamma$ [56], $H \rightarrow hh \rightarrow b\bar{b}\gamma\gamma$ [57] and $H \rightarrow hh \rightarrow b\bar{b}b\bar{b}$ [58]. Heavy SM-like Higgs bosons decaying to pair of W bosons with final state consisting of one lepton, two jets and missing transverse energy has been studied by the CMS collaboration [59]. Heavy pseudoscalar Higgs boson (A) decaying to a Z boson and a light Higgs boson h has also been searched by both the ATLAS and CMS collaborations at 19.7 fb^{-1} luminosity at the 8 TeV run of LHC [60, 61]. In addition, search for the charged Higgs bosons (H^\pm) decaying to $\tau\nu_\tau$, $c\bar{s}$ and $t\bar{b}$ are also performed at the LHC when H^\pm are produced via $t\bar{t}$ or in association with top quarks [62, 66]. So far, the ATLAS and CMS data have not revealed any clear signature of the signal and thus they put model-independent 95% C.L. upper limits on the production cross section times branching ratios for different production processes and decay modes.

In the MSSM, the couplings of h with the SM electro-weak gauge bosons are proportional to $\sin(\beta - \alpha)$. Now, the measured values of the couplings of the observed 125 GeV Higgs boson with the SM W/Z bosons are quite consistent with the SM expectations, which thus restricts the value of $\sin(\beta - \alpha)$ near to unity. Besides, non observation of additional Higgses (H , A and H^\pm) at the LHC implies that their masses are possibly well above the electro-weak scale. One can satisfy both the above-mentioned observations in the MSSM by choosing $\alpha \sim 0$ and $\beta \sim \frac{\pi}{2}$ and/or $M_A \gg M_Z$, which is generally known as the decoupling limit of the MSSM [20]. In this paper, however, we would like to address the following question: Is there any MSSM parameter space still allowed by the current LHC data where one can expect to have moderate Higgs mixing angle (α) with relatively light (say, hundred to few hundred GeV) additional Higgses? In other words, we are looking for a feasible MSSM parameter space where the non-negligible Higgs mixing still exists, and simultaneously we have light additional scalar particles which can be probed at the run-II of LHC. Our strategy can be summarized as follows:

- We first perform a global χ^2 analysis by scanning the relevant parameters of the MSSM Higgs sector and incorporating the updated Higgs signal strengths from the ATLAS, CMS and Tevatron experiments. The constraints coming from the precision measurements of rare decays like $B_s \rightarrow \mu^+ \mu^-$ and $b \rightarrow s\gamma$ are also considered.
- We then impose the LHC direct search bounds on the heavy scalar/pseudoscalar Higgs (H/A) and charged Higgs boson (H^\pm) masses and various branchings in the allowed parameter space.
- Finally, we study the possibility to probe the remaining parameter space in the high luminosity run of LHC.

In Sec. 2, we discuss the detailed prescription of our global fit analysis, followed by a brief outline of our parameter space scan. The favorable parameter space obtained after the global analysis is discussed in Sec. 2.2. In Sec. 3, we present the current limits on production cross section times branching ratios obtained from the direct search of both neutral and charged Higgs bosons at the LHC. Future limits for the high luminosity run of LHC are discussed in Sec. 4. Finally in Sec. 5 we summarize our results.

2 Global analysis and available pMSSM parameter space

In this section, we discuss the details of our global fit analysis. Current bounds on various Higgs coupling measurements by the ATLAS and CMS collaborations at the LHC, and also by the CDF and $D\bar{0}$ collaborations at the Tevatron experiment are considered as the inputs to our global analysis. We also consider two important flavour physics constraints, namely $\text{Br}(b \rightarrow s\gamma)$ and $\text{Br}(B_s \rightarrow \mu^+ \mu^-)$ [67]. Finally, we discuss the features of the available parameter space satisfying the updated Higgs and flavour physics data.

2.1 Experimental inputs and Global fit analysis

Both the ATLAS and CMS collaborations have published the results of the 125 GeV Higgs boson searches combining the 7+8 TeV data at the end of 8 TeV run of LHC [6–17]. Besides, the results of the SM Higgs boson search by the CDF and $D\bar{0}$ collaborations at the Tevatron experiment are also available in the literature [3, 68]. In our global analysis, we consider the most updated Higgs data obtained from the LHC and Tevatron experiments. The Higgs bosons are produced at the LHC mainly via the gluon-gluon fusion (ggF) process. However, there exist other sub-dominant production mechanisms e.g., vector boson fusion (VBF), associated production with a W/Z boson (Vh), associated production with a pair of top quarks ($t\bar{t}h$). The decay modes of the Higgs boson which are analyzed by the ATLAS and CMS collaborations are $h \rightarrow \gamma\gamma$ [6, 7], $h \rightarrow WW^*$ [8, 9], $h \rightarrow ZZ^*$ [10, 11], $h \rightarrow b\bar{b}$ [12, 13], and $h \rightarrow \tau^+ \tau^-$ [14, 15], while the CDF and $D\bar{0}$ collaborations

have analyzed the $\gamma\gamma$, WW^* and $b\bar{b}$ decay modes of the Higgs boson [3, 68]. The experimental findings are usually presented in terms of the signal strength variable (μ), which is defined as the ratio of the production cross section (σ) times the branching ratio (Br) to a specific decay mode for a given new physics model normalized to the SM prediction. For example, when the Higgs boson is produced via gluon-gluon fusion process and it decays to a generic final state $X\bar{X}$ ($\gamma\gamma$, WW^* , ZZ^* , $b\bar{b}$ and $\tau^+\tau^-$), then one can define the signal strength variable μ , assuming narrow-width approximation, as:

$$\mu_{ggF}(X\bar{X}) = \frac{\Gamma(h \rightarrow gg)}{\Gamma(h_{SM} \rightarrow gg)} \times \frac{Br(h \rightarrow X\bar{X})}{Br(h_{SM} \rightarrow X\bar{X})}, \quad (1)$$

where h is a observed 125 GeV Higgs boson and h_{SM} is the SM Higgs boson. Similarly, if the Higgs boson is produced via VBF fusion process and it decays to $X\bar{X}$, then one can define,

$$\mu_{VBF/VH}(X\bar{X}) = \frac{\Gamma(h \rightarrow WW)}{\Gamma(h_{SM} \rightarrow WW)} \times \frac{Br(h \rightarrow X\bar{X})}{Br(h_{SM} \rightarrow X\bar{X})}. \quad (2)$$

From Eq. 1 and 2 it is evident that the signal strengths are functions of the partial decay widths and the total decay width of the Higgs boson. The presence of new particles/interactions in the new physics models leads to modifications in the partial/total decay widths, and thereby changes in the value of signal strength variable. Thus, precise measurements of these signal strength variables are extremely crucial as a small but statistically significant deviation from the SM expectation will hint at possible signatures of the new physics. Note that, in the timeline of the Moriond 2014 [69] workshop to the end of December 2014, significant changes have been observed in the measurement of various Higgs signal strengths. For example, ATLAS data for di-photon signal strength has changed from $1.57^{+0.33}_{-0.28}$ [69] to 1.17 ± 0.27 [6], while the same from the CMS has changed from 0.77 ± 0.27 [69] to $1.14^{+0.26}_{-0.23}$ [7]. Besides, both statistical and systematics uncertainties associated to some of these signal strengths have been reduced after the combination of (7+8) TeV LHC data. Near the end of last year, the CDF and $D\bar{0}$ collaborations have also updated the constraints of 125 GeV Higgs boson couplings to fermions and vector bosons. In this work, we perform a global analysis considering all these most updated Higgs signal strengths as of the end of 2014. The available signal strength variables², for different production and decay modes of the Higgs boson at the LHC are summarized in Table 1 to Table 5 while Tevatron Higgs data is shown in Table 6.

Let us now discuss the details of the MSSM parameter space scan. We do not consider any specific SUSY breaking scenario, rather we focus on the generic phenomenological MSSM (pMSSM) model with 19 free parameters and perform a random scan for approximately 100 million points. Those parameters that are relevant to the MSSM Higgs sector, namely pseudo-scalar mass parameter M_A , the ratio of the vacuum expectation values of two Higgs doublets $\tan\beta$, higgsino

²For global fit analysis, we consider the signal strengths for different production modes as presented for individual decay channels. In other words, we do not consider the inclusive results for a given decay mode.

Channel	Signal strength (μ)		Production mode		
	<i>ATLAS</i>	<i>CMS</i>	ggF	VBF	Vh
$\mu(ggh)$	1.32 ± 0.38	$1.12^{+0.37}_{-0.32}$	100%	-	-
$\mu(VBF)$	0.8 ± 0.7	$1.58^{+0.77}_{-0.68}$	-	100%	-
$\mu(Wh)$	1.0 ± 1.6	$-0.16^{+1.16}_{-0.79}$	-	-	100%
$\mu(Zh)$	$0.1^{+3.7}_{-0.1}$	-	-	-	100%

Table 1: Signal strengths of $h \rightarrow \gamma\gamma$ channel as recorded by the ATLAS [6] and CMS [7] collaborations after 7+8 TeV run of LHC with 25 fb^{-1} of luminosity. The amount of contribution to a given channel from each production modes are shown in Column 4-6. The total χ^2 for the $\gamma\gamma$ channel with respect to the SM is $= 0.85$ (ATLAS) + 1.868 (CMS) $= 2.718$.

Channel	Signal strength (μ)		Production mode		
	<i>ATLAS</i>	<i>CMS</i>	ggF	VBF	Vh
$\mu(ggh + b\bar{b}h + t\bar{t}h)$	$1.66^{+0.51}_{-0.44}$	$0.80^{+0.46}_{-0.36}$	100%	-	-
$\mu(VBF + Vh)$	$0.26^{+1.64}_{-0.94}$	$1.7^{+2.2}_{-2.1}$	-	60%	40%

Table 2: Signal strengths of $h \rightarrow ZZ^*$ channel as recorded by the ATLAS [10] and CMS [11] collaborations after 7+8 TeV run of LHC with 25 fb^{-1} of luminosity. The amount of contribution to a given channel from each production modes are shown in Column 4-6. The total χ^2 for the ZZ^* channel with respect to the SM is $= 2.493$ (ATLAS) + 0.3 (CMS) $= 2.793$.

Channel	Signal strength (μ)		Production mode		
	<i>ATLAS</i>	<i>CMS</i>	ggF	VBF	Vh
$\mu(ggF)$	$1.02^{+0.29}_{-0.26}$	-	100%	-	-
$\mu(VBF)$	$1.27^{+0.53}_{-0.45}$	-	-	100%	-
$\mu(0/1 \text{ jet})$	-	$0.74^{+0.22}_{-0.20}$	97%	3%	-
$\mu \text{ (VBF tag)}$	-	$0.60^{+0.57}_{-0.46}$	17%	83%	-
$\mu \text{ (Vh tag (} 2l2\nu2j))$	-	$0.39^{+1.97}_{-1.87}$	-	-	100%
$\mu \text{ (Wh tag(} 3l3\nu))$	-	$0.56^{+1.27}_{-0.95}$	-	-	100%

Table 3: Signal strengths of $h \rightarrow WW^*$ channel as recorded by the ATLAS [8] and CMS [9] collaborations after 7+8 TeV run of LHC with 25 fb^{-1} of luminosity. The amount of contribution to a given channel from each production modes are shown in Column 4-6. The total χ^2 for the WW^* channel with respect to the SM is $= 0.366$ (ATLAS) + 2.104 (CMS) $= 2.470$.

Channel	Signal strength (μ)		Production mode		
	<i>ATLAS</i>	<i>CMS</i>	ggF	VBF	Vh
$\mu(\text{Vh tag})$	$0.51^{+0.40}_{-0.37}$	1.0 ± 0.5	-	-	100%

Table 4: Signal strengths of $h \rightarrow b\bar{b}$ channel as recorded by the ATLAS [12] and CMS [13] collaborations after 7+8 TeV run of LHC with 25 fb^{-1} of luminosity. The amount of contribution to a given channel from each production modes are shown in Column 4-6. The total χ^2 for the $b\bar{b}$ channel with respect to the SM is $= 1.50$ (ATLAS) $+ 0.0$ (CMS) $= 1.5$.

Channel	Signal strength (μ)		Production mode		
	<i>ATLAS</i>	<i>CMS</i>	ggF	VBF	Vh
$\mu(ggF)$	$1.93^{+1.45}_{-1.15}$	-	100 %	-	-
$\mu(VBF + Vh)$	$1.24^{+0.58}_{-0.54}$	-	-	60%	40%
μ (0-jet)	-	0.34 ± 1.09	96.9%	1.0%	2.1
μ (1-jet)	-	1.07 ± 0.46	75.7%	14%	10.3
μ (VBF tag)	-	0.94 ± 0.41	19.6	80.4	-
μ (Vh tag)	-	-0.33 ± 1.02	-	-	100%

Table 5: Signal strengths of $h \rightarrow \tau^+\tau^-$ channel as recorded by the ATLAS [14] and CMS [15] collaborations after 7+8 TeV run of LHC with 25 fb^{-1} of luminosity. The amount of contribution to a given channel from each production modes are shown in Column 4-6. The total χ^2 for the $\tau^+\tau^-$ channel with respect to the SM is $= 0.857$ (ATLAS) $+ 2.11$ (CMS) $= 2.967$.

Channel	Signal strength (μ)	Production mode		
	<i>Tevatron</i>	ggF	VBF	Vh
$\mu(H \rightarrow \gamma\gamma)$	$6.14^{+3.25}_{-3.19}$	78%	5%	17%
$\mu(H \rightarrow WW^*)$	$0.85^{+0.88}_{-0.81}$	78%	5%	17%
$\mu(H \rightarrow b\bar{b})$	$1.59^{+0.69}_{-0.72}$	-	-	100%

Table 6: Signal strengths of $h \rightarrow \gamma\gamma$, WW^* , and $b\bar{b}$ channel as recorded by the CDF and $D\emptyset$ collaborations at the Tevatron with 10 fb^{-1} of luminosity at $\sqrt{s} = 1.96 \text{ TeV}$ [3, 68]. The amount of contribution to a given channel from each production modes are shown in Column 4-6. The total χ^2 for the above three modes with respect to the SM is $= 3.296$.

mass parameter μ , the third generation squark trilinear couplings A_t and A_b (trilinear couplings of sleptons and first two generations squarks are set to zero), third generation squark soft mass

parameters M_{Q3} , M_{U3} and M_{D3} , are scanned in the following ranges:

$$\begin{aligned} 1 < \tan \beta < 50, \quad 100 \text{ GeV} < M_A < 600 \text{ GeV}, \\ -8000 \text{ GeV} < A_t, A_b < 8000 \text{ GeV}, \quad 100 \text{ GeV} < \mu < 8000 \text{ GeV}, \\ 100 \text{ GeV} < M_{Q3}, M_{U3} < 8000 \text{ GeV}, \quad 100 \text{ GeV} < M_{D3} < 8000 \text{ GeV}, \end{aligned} \quad (3)$$

while we fix the following parameters since they have little impact on our analysis,

$$\begin{aligned} M_1 &= 100 \text{ GeV}, \quad M_2 = 2000 \text{ GeV}, \quad M_3 = 3000 \text{ GeV}, \\ M_{L_{1,2,3}} &= M_{E_{1,2,3}} = 3000 \text{ GeV}, \quad M_{Q_{1,2}} = 3000 \text{ GeV}, \quad M_{U_{1,2}} = M_{D_{1,2}} = 3000 \text{ GeV}, \end{aligned} \quad (4)$$

where $M_{1,2,3}$ are the gaugino mass parameters, M_{L_i} and M_{E_i} ($i = 1, 2, 3$) are the left and right handed slepton soft SUSY breaking mass parameters, and M_{Q_i} , M_{U_i} , M_{D_i} ($i = 1, 2$) are the first two generation squark soft SUSY breaking mass parameters.

We scan the third generation trilinear couplings (A_t and A_b) and soft masses (M_{Q3} , M_{U3} , M_{D3}) over a wide range in order to obtain the lightest MSSM Higgs boson mass in the range of 125 ± 3 GeV assuming 3 GeV uncertainty in Higgs mass calculation [70]. Since we are interested in the possibility of having light additional Higgses, we restrict M_A up to 600 GeV. From the above choices of the model parameters, it is evident that we do not consider the possibility of the decay of h to MSSM particles. We use SUSPECT (version 2.43) [71] to scan the MSSM parameter space and SuperIso (version 3.4) [72] to calculate the flavour physics observables, while the branching ratios of the lightest Higgs boson are evaluated using HDECAY (version 6.41) [73].

Now, to combine the available information on different signal strength variables from the ATLAS, CMS and Tevatron, and to compare with the MSSM expectations, we compute χ^2 for all the scanned parameter space points, defined as below:

$$\chi^2 = \sum_i \frac{(\bar{\mu}_i - \mu_i)^2}{\Delta\mu_i^2}, \quad (5)$$

where μ_i is the experimentally observed signal strength for a particular production/decay mode i , and $\bar{\mu}_i$ is the value predicted for the same channel for a chosen MSSM parameter space point with $\Delta\mu_i$ being the measure of the experimental error associated to that channel. The sum over i takes into account of all the experimentally measured production and decay modes of the Higgs boson.

It is to be noted that, different production processes can, in principle, contribute to a particular experimental search channel, thereby while calculating the signal strengths for a parameter space point, contributions coming from different production processes need to be considered. Following the procedure of Ref. [29], we implement this modification in our analysis as follows:

$$\bar{\mu}_i = \sum T_i^j \hat{\mu}_j, \quad (6)$$

where T_i^j denotes the amount of contribution that can originate from the production mode j to the category/channel i with $\hat{\mu}_i$ being the signal strength corresponding to the MSSM parameter

space point. For example, the category $\mu(\text{VBFtag})$, as introduced in Table 3, receives 17% and 83% contributions from the ggF and VBF processes respectively [74]. So, we calculate $\hat{\mu}_{ggF}$ and $\hat{\mu}_{VBF}$, and then scale them with 0.17 and 0.83 (the T_i^j s here) respectively to obtain the proper signal strength ($\bar{\mu}$) corresponding to VBFtag category. To obtain the contributions coming from different production processes to a given decay mode/category, we use LHC Higgs cross section working group report [74].

We consider altogether 28 data points (i.e., experimental inputs, see Table 1 - 6) combining the CMS and ATLAS and Tevatron Higgs data. We calculate χ^2 for all the scanned parameter space points and find the minimum of χ^2 . We call this minimum as the *approximate* minima (χ_{approx}^2). In order to obtain the *true* χ^2 minimum (χ_{min}^2), we vary the parameters around their *approximated* values i.e., values corresponding to the approximate χ^2 minimum. We present the parameter space that is available after the global analysis considering the 1σ and 2σ intervals with $\chi^2 = \chi_{\text{min}}^2 + 2.3$ and $\chi^2 = \chi_{\text{min}}^2 + 6.18$ respectively in $M_A - \tan\beta$ plane [75]. The “best fit” value corresponds to $M_A \sim 584$ GeV and $\tan\beta \sim 36$. To determine how a set of experimental data is well represented by any given model, one usually calculates the chi-square per degrees of freedom (d.o.f) i.e., $\chi^2/\text{d.o.f}$. The minimum value of χ^2 obtained from the analysis for SM is 15.744 with $\chi^2/\text{d.o.f} = \chi^2/28 = 0.562$, while for MSSM we obtain $\chi_{\text{min}}^2 = 15.013$ with $\chi^2/\text{d.o.f} = \chi^2/20 = 0.75$.

2.2 Available MSSM parameter space

Before we proceed to discuss our findings, let us review our methodology once more. We first perform a χ^2 analysis using a random scan of the parameters relevant to the MSSM Higgs sector, then we find the true χ_{min}^2 to get the “best-fit” values of those parameters. The points with χ^2 within 2σ of the true χ_{min}^2 are only considered for further analysis. We impose the two most stringent rare b-decay constraints, namely $\text{Br}(b \rightarrow s\gamma)$ and $\text{Br}(B_s \rightarrow \mu^+\mu^-)$, and allow 2σ deviation³ [67],

$$\begin{aligned} 2.82 \times 10^{-4} < \text{Br}(B_s \rightarrow X_s\gamma) < 4.04 \times 10^{-4} \\ 1.57 \times 10^{-9} < \text{Br}(B_s \rightarrow \mu^+\mu^-) < 4.63 \times 10^{-9}. \end{aligned} \quad (7)$$

In Fig.1, we show the parameter space in the $M_A - \tan\beta$ plane obtained from the global fit analysis and also satisfying the flavour physics constraints. Magenta (black) coloured triangle (circle) shaped points represent 2σ (1σ) allowed parameter space. The region with $M_A \leq 350$ GeV and $\tan\beta \geq 25$ are excluded by the stringent $\text{Br}(B_s \rightarrow \mu^+\mu^-)$ constraint, which is expected to dominate for regions with large $\tan\beta$ and relatively smaller M_A . However, for significantly larger M_A i.e., $M_A \geq 425$ GeV, the effect of this constraint is negligible. Besides, most of the points in the region with $M_A \leq 350$ GeV with $\tan\beta \leq 8$ are excluded by the $\text{Br}(b \rightarrow s\gamma)$ constraint.

³The current measurements of these two b-observables are $\text{Br}(B_s \rightarrow X_s\gamma) = 3.43 \pm 0.22 \pm 0.21(\text{theo.})$ and $\text{Br}(B_s \rightarrow \mu^+\mu^-) = 3.1 \pm 0.7 \pm 0.31(\text{theo.})$ [67]. We follow Ref. [76] for the conservative estimates of the theoretical uncertainties associated to these two flavor observables.

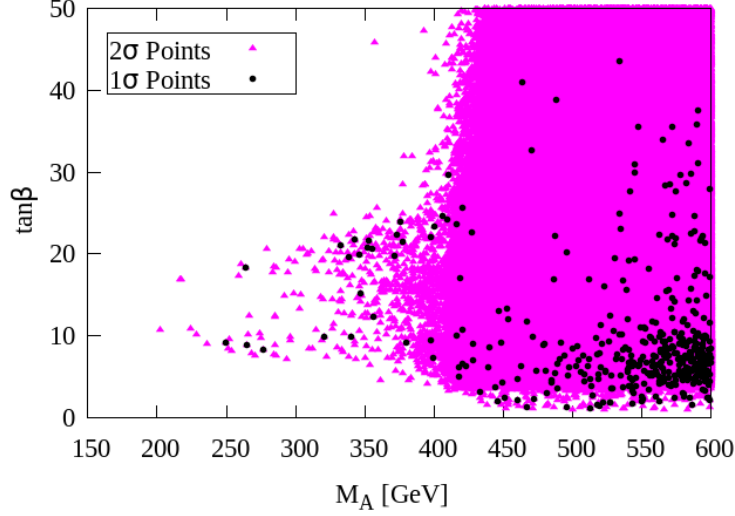


Figure 1: *Parameter space allowed in $M_A - \tan\beta$ plane from our global fit analysis and also satisfying the flavour physics constraints on $Br(b \rightarrow s\gamma)$ and $Br(B_s \rightarrow \mu^+\mu^-)$. Magenta (black) coloured triangle (circle) shaped points represent 2σ (1σ) allowed parameter space from global fits of 125 GeV Higgs data after Run-I of LHC. In rest of our analysis, while presenting the direct search constraints and the future limits on the heavy Higgs masses and BRs, we would consider these 2σ points which satisfies our global fit analysis and the updated flavour data.*

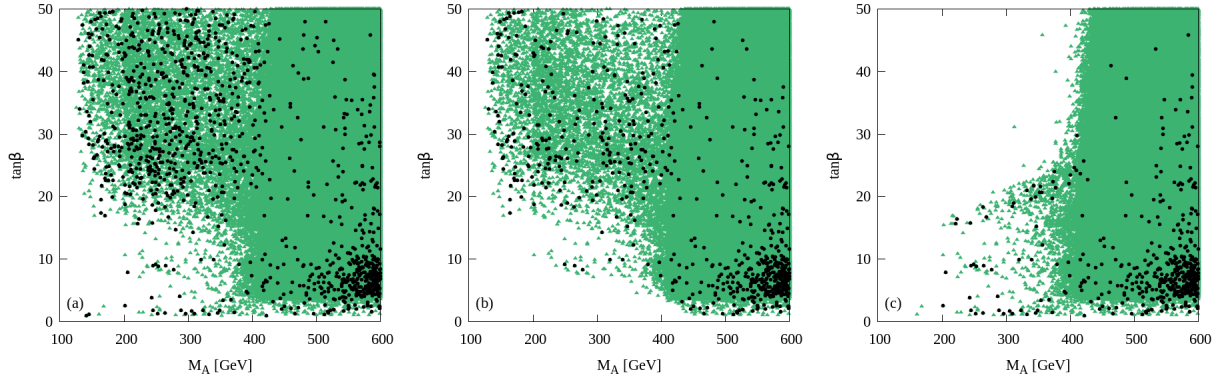


Figure 2: *Scatter plots in the (a) $M_A - \tan\beta$ plane without any flavor constraint (left panel), (b) $M_A - \tan\beta$ plane only after imposing $Br(b \rightarrow s\gamma)$ constraint (middle panel) and (c) $M_A - \tan\beta$ plane after imposing only $Br(B_s \rightarrow \mu^+\mu^-)$ constraint (right panel). In Fig. 1, we show the same correlation after the imposition of both $Br(b \rightarrow s\gamma)$ and $Br(B_s \rightarrow \mu^+\mu^-)$ constraints.*

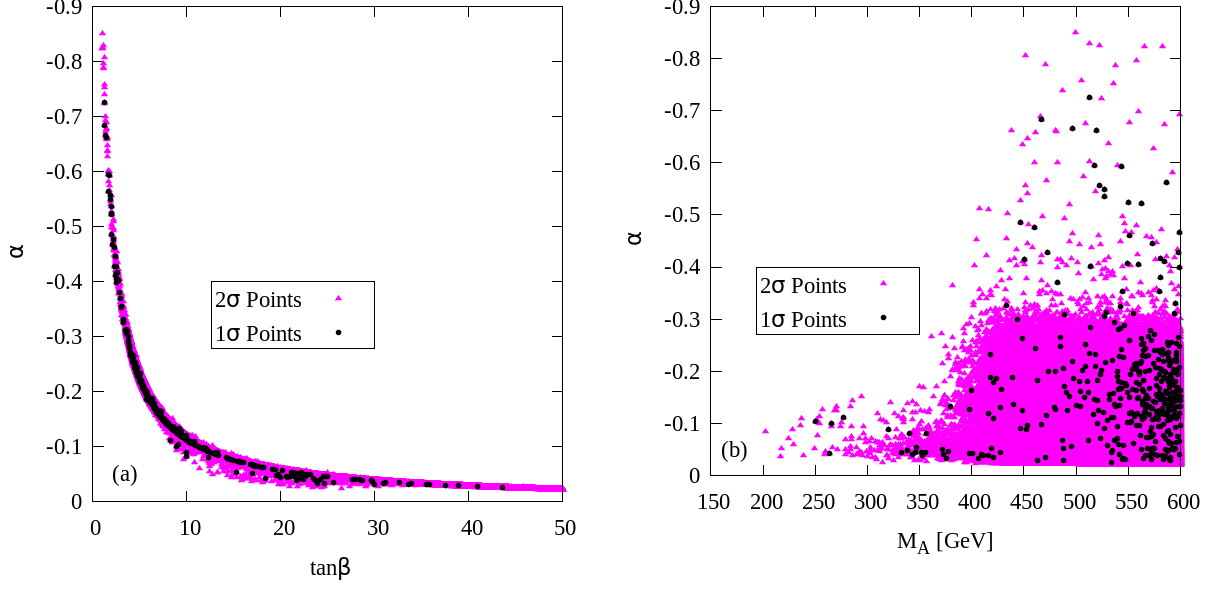


Figure 3: Left panel (a) shows the allowed parameter space in $\tan\beta - \alpha$ plane after the global fit analysis and also satisfying the flavour physics constraints. Colour conventions are same as Fig. 1. In the right panel (b), we display the same allowed parameter space but now is presented in the $M_A - \alpha$ plane.

In order to display the interplay of two flavour physics constraints, in Fig. 2(a) we first show the parameter space obtained after the global analysis with Higgs mass constraint ($122 \text{ GeV} \leq M_h \leq 128 \text{ GeV}$) only, without imposing any flavor physics constraint. In the middle panel (b), we then show the same distribution but only after imposing the $\text{Br}(b \rightarrow s\gamma)$ constraint. In right-most figure (Fig. 2c) we plot the same correlation with imposing $\text{Br}(B_s \rightarrow \mu^+\mu^-)$ constraint only. The effect of the $\text{Br}(B_s \rightarrow \mu^+\mu^-)$ constraint in the low M_A and large $\tan\beta$ region, and the impact of $\text{Br}(b \rightarrow s\gamma)$ in low M_A and low $\tan\beta$ is now clearly visible from these plots. Once we impose both the Higgs mass and flavour physics constraints, the available parameter space has already been shown in Fig. 1. Note that, in rest of our analysis, we name these 2σ allowed points collectively as the “scanned data set” and present the direct search constraints and the future limits on the heavy Higgs masses and couplings using this data set.

In Fig. 3, we show the scatter plots in the (a) $\alpha - \tan\beta$ and (b) $\alpha - M_A$ planes, where α is the Higgs mixing angle. But, before we proceed, let’s first briefly discuss the idea of the “alignment limit” (for details see Refs. [77–80]). In the MSSM, the couplings (at the tree level) of the CP-even

Higgs bosons (h, H) to SM gauge bosons are [20],

$$\begin{aligned} g_{hVV} &= \sin(\beta - \alpha) g_V \\ g_{HVV} &= \cos(\beta - \alpha) g_V, \end{aligned} \quad (8)$$

while, couplings to the SM fermions are [20],

$$\begin{aligned} g_{hdd} &= -\sin \alpha / \cos \beta g_f = (\sin(\beta - \alpha) - \tan \beta \cos(\beta - \alpha)) g_f \\ g_{huu} &= -\cos \alpha / \sin \beta g_f = (\sin(\beta - \alpha) + \cot \beta \cos(\beta - \alpha)) g_f \\ g_{Hdd} &= -\cos \alpha / \cos \beta g_f = (\cos(\beta - \alpha) + \tan \beta \sin(\beta - \alpha)) g_f \\ g_{Huu} &= -\sin \alpha / \sin \beta g_f = (\cos(\beta - \alpha) - \cot \beta \sin(\beta - \alpha)) g_f, \end{aligned} \quad (9)$$

where g_V and g_f are the corresponding SM couplings with $g_V = 2iM_V^2/v$ and $g_f = iM_f/v$ for a generic gauge boson V ($V \equiv W, Z$) and a fermion f with $v = 246$ GeV. Now, the alignment limit is the limiting case when the lightest CP-even Higgs boson mimic the properties of the SM Higgs and the SM gauge bosons couple to the light CP-even Higgs boson only (i.e., $g_{hVV} \sim 1$ and $g_{HVV} \sim 0$). This limit can be easily achieved with the variation of the two quantities α and β . For example, let's assume a special case: $(\beta - \alpha) \sim \pi/2$ for some specific choices of α and β , then the couplings of the lightest CP even Higgs boson to the SM gauge bosons are SM-like, while heavier CP even Higgs boson couplings become highly suppressed. Note that, even though the heavier CP even Higgs has highly suppressed coupling to the SM gauge bosons, however it can have non-zero couplings to the SM fermions depending on the choice of $\tan \beta$ (see Eq. 9). Now, let's discuss how we achieve the alignment limit from our parameter space scan. To do so, let's first divide the region of interest into three parts, namely $\tan \beta < 5$, $5 < \tan \beta < 20$, and $\tan \beta > 20$. The region with $\tan \beta < 5$ corresponds to $\alpha > -0.2$ radian. Now, $\tan \beta = 5$ implies $\beta = 1.373$ radian, which means $(\beta - \alpha) = 1.573$ radian or, around 90 degree with $\alpha = -0.2$ radian, so here we are near the alignment limit ($\beta - \alpha = \pi/2$) [77]. The region with $\tan \beta > 20$ corresponds to very small α (< -0.05 radian), and thereby $(\beta - \alpha) \sim \pi/2$ i.e., we again achieve the alignment limit. The intermediate regime with $5 < \tan \beta < 20$ also satisfies the criteria of alignment. However, we see that in this alignment limit, M_A can be as light as 300 - 400 GeV with relatively large α (see Fig. 3(b)) satisfying current data. This scenario can be thought of as the ‘‘alignment without decoupling’’ scenario, as discussed in Ref. [78–80]. In fact, in order to make a more quantitative statement, In Fig. 4 we present the allowed parameter space in the $(\beta - \alpha) - \tan \beta$ plane with different choices of M_A . We divide the entire M_A region into four parts: $200 < M_A < 300$ GeV (red/square), $300 < M_A < 400$ GeV (black/circle), $400 < M_A < 500$ GeV (green/triangle), and $500 < M_A < 600$ GeV (blue/cross), while the red horizontal line at $(\beta - \alpha) = 1.571$ indicates the exact value at the alignment limit. From Fig. 3 and Fig. 4 it is clear that regions with light M_A (≤ 400 GeV) satisfying the alignment limit is perfectly allowed by the current data, one is thus not always forced to be in the decoupling limit to comply with LHC data.

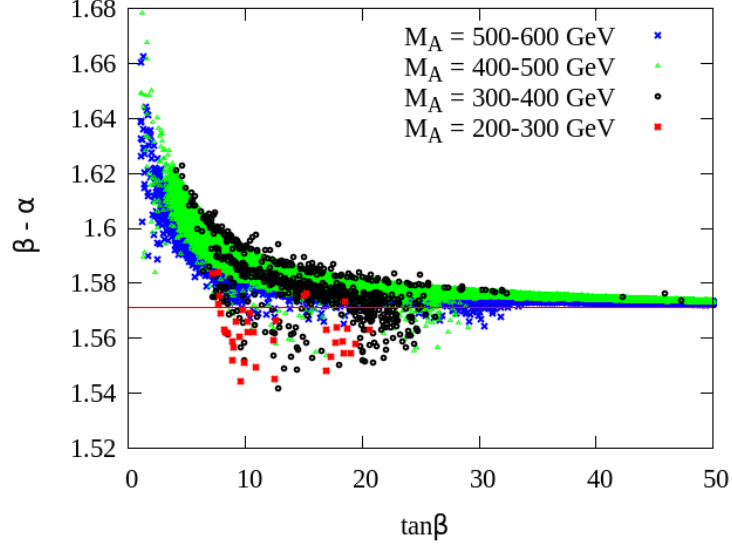


Figure 4: The allowed parameter space in the $(\beta - \alpha) - \tan\beta$ plane is presented with different choices of M_A . The entire M_A region is divided in four parts, namely $200 < M_A < 300$ GeV (red/square), $300 < M_A < 400$ GeV (black/circle), $400 < M_A < 500$ GeV (green/triangle), and $500 < M_A < 600$ GeV (blue/cross). The red horizontal line at $(\beta - \alpha) = 1.571$ indicates the value of $(\alpha - \beta)$ at the alignment limit. We see that regions with light M_A (≤ 400 GeV) satisfying the alignment limit are perfectly allowed by the current data.

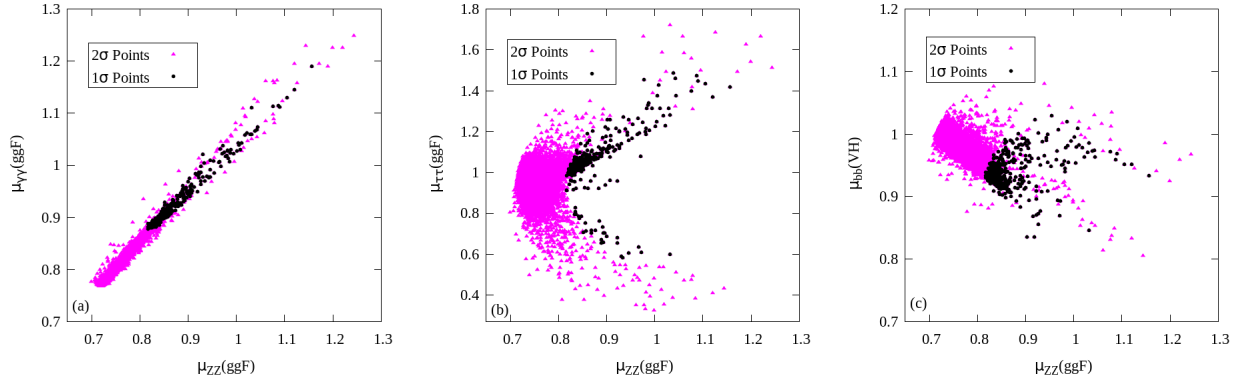


Figure 5: Signal strength correlations in (a) $\mu_{ZZ} - \mu_{\gamma\gamma}$, (b) $\mu_{ZZ} - \mu_{\tau^+\tau^-}$ and (c) $\mu_{ZZ} - \mu_{b\bar{b}}$ planes. Magenta (black) coloured triangle (circle) shaped points represent 2σ (1σ) allowed points of our “scanned data set”.

Before we end this section, we would like to discuss the correlations of various Higgs signal strength variables. In Fig. 5, we show the scatter plots in $\mu_{ZZ} - \mu_{\gamma\gamma}$ (left), $\mu_{ZZ} - \mu_{\tau^+\tau^-}$ (middle)

and $\mu_{ZZ} - \mu_{bb}$ (right) planes. We find that the partial widths $\Gamma(h \rightarrow ZZ)$ and $\Gamma(h \rightarrow WW)$ remain almost unaltered with respect to the SM values, however $\Gamma(h \rightarrow b\bar{b})$ and total decay width of Higgs (Γ_{tot}) have increased while $\Gamma(h \rightarrow gg)$ has decreased for most of the scanned data points. Now, we know that when the total decay width increases, the branching ratios of various sub-leading decay modes like $\gamma\gamma$, gg , ZZ , WW decreases. Hence, the suppression in the $\mu_{ZZ}/\mu_{\gamma\gamma}$ can be thought of as the interplay of two effects: the increase in total decay width (or, decrease in $h \rightarrow ZZ$ or $h \rightarrow \gamma\gamma$ branching ratios) and decrease in $\Gamma(h \rightarrow gg)$ with respect to the SM. Now, in order to understand the bb and $\tau\tau$ correlations in Fig. 5(b) and Fig. 5(c), we need to discuss the couplings of the lightest CP-even Higgs boson with the b quark and τ lepton. At the tree level, the Yukawa couplings of b and τ are proportional to $\frac{\sin \alpha}{\cos \beta}$ (see Eq. 9). However, loop corrections (in powers of $\alpha_s \tan \beta$) involving heavier supersymmetric particles can significantly modify the b quark mass and its Yukawa coupling from its tree level predictions. In an effective Lagrangian approach, these effects are parametrized by the quantity Δ_b and one can write [81–84],

$$L_{hb\bar{b}} = -\frac{m_b}{v_{SM}} \left(\frac{1}{1 + \Delta_b} \right) \left(-\frac{\sin \alpha}{\cos \beta} \right) \left(1 - \frac{\Delta_b}{\tan \beta \tan \alpha} \right) b\bar{b}h \quad (10)$$

where $v_{SM} = (\sqrt{2}G_F)^{-1/2}$. The bottom quark mass can now be written as,

$$m_b \rightarrow \frac{y_b v_1}{\sqrt{2}} (1 + \Delta_b), \quad (11)$$

where $v_1 = v_{SM} \cos \beta$ and y_b the bottom Yukawa coupling. In order to understand various terms of Eq. 10, in Fig. 6(a), we show the distribution of the quantity,

$$\epsilon = \left(\frac{1}{1 + \Delta_b} \right) \times \left(1 - \frac{\Delta_b}{\tan \beta \tan \alpha} \right) \quad (12)$$

with respect to Δ_b for all the 2σ (magenta triangle) and 1σ (black circles) allowed points. It is evident from the figure that for significant number of points, Δ_b is mostly positive and varies within 10-15%. However, the effect of this variation of Δ_b on ϵ is small. Thus, we understand that Δ_b is not playing a very significant role here, and so we then proceed to estimate the individual quantities that are involved in $\mu_{\tau\tau}$ and μ_{bb} . From Eq. 1 and Eq. 2, we find that the quantities of interest are $\Gamma(h \rightarrow gg)$, $\Gamma(h \rightarrow WW)$, $BR(h \rightarrow ZZ)$, $BR(h \rightarrow \tau\tau)$ and $BR(h \rightarrow b\bar{b})$. In Fig. 6(b), we display the variation of the ratio of partial widths of Higgs to $b\bar{b}$ and $\tau\tau$ with respect to the SM values with the tree level coupling $\frac{\sin \alpha}{\cos \beta}$. For most of the 2σ allowed points, we find 25 - 30% enhancement in bb and $\tau\tau$ partial widths (see Fig. 6(b)), however we check that $\Gamma(h \rightarrow ZZ)$ remains unaltered. Thus, increase in $\Gamma(h \rightarrow b\bar{b})$ and thereby increase in Γ_{tot} results in 20-25% modifications in $BR(h \rightarrow \tau\tau)$, however, being the dominant decay mode, change in $BR(h \rightarrow b\bar{b})$ is small (see Fig. 6(c)). Thus, one can conclude that the larger spread in $\mu_{\tau\tau}$ as seen in Fig. 5(b) compared to Fig. 5(c) is coming from the interplay of the total Higgs decay width and individual Higgs branching ratios along with a mild dependence of Δ_b .

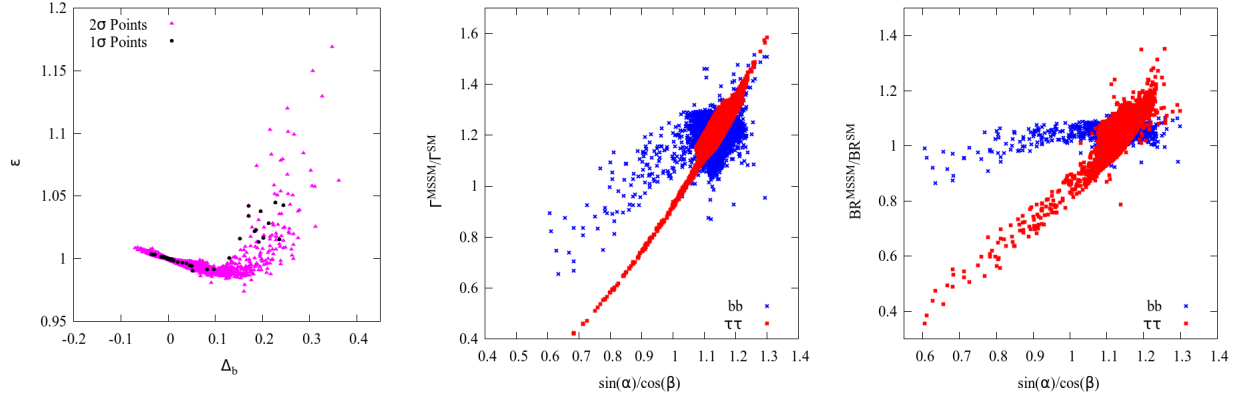


Figure 6: Left panel shows the distribution of the quantity $\epsilon = \left(\frac{1}{1+\Delta_b}\right) \times \left(1 - \frac{\Delta_b}{\tan \beta \tan \alpha}\right)$ with the variation of Δ_b . The variation of the ratios of the partial decay widths and branching ratios of the Higgs boson to the SM values for the $b\bar{b}$ and $\tau^+\tau^-$ modes with the tree level Higgs Yukawa couplings $\frac{\sin \alpha}{\cos \beta}$ are shown in the middle and right panel respectively. For more details, see the text.

3 Bounds on MSSM heavy Higgses from direct searches

In the previous section, we first describe the global fit analysis, and then show that the signal strength measurements of the SM-like Higgs boson with different possible final state signatures do not exclude the possibility of having additional light Higgses (say ≤ 600 GeV) with moderate values of Higgs mixing angle α . One can now ask whether these light MSSM Higgses are still allowed satisfying the direct search bounds at the LHC-8, which is precisely the goal of this section. Here we will impose the bounds set by the ATLAS and CMS collaborations on the masses and branching ratios of the neutral and charged Higgs bosons at the end of 8 TeV run of LHC. We calculate the production cross section of the neutral heavy Higgses (H and A) using SuShi (version 1.4.1) [85] and charged Higgs (H^\pm) using PYTHIA (version 6.4.28) [86]. The branching ratios of both the charged and neutral Higgses are evaluated using HDECAY (version 6.41) [73].

3.1 Neutral Higgs boson searches

3.1.1 Search for H with $\gamma\gamma$ final states

The di-photon invariant mass distribution plays an important role to discover the 125 GeV Higgs boson at the LHC. However, the sensitivity of this channel falls rapidly with the increase of the SM Higgs boson mass and become vanishingly small beyond 150 GeV [56]. In models with additional Higgses, di-photon mode can be a useful probe to search for these heavy resonances. The CMS collaboration has searched for the CP-even heavy MSSM Higgs H using the di-photon invariant

mass distribution with 19.7 fb^{-1} of data at the 8 TeV run of LHC. They assume that the Higgs is produced via gluon-gluon fusion process. Both narrow and wide width heavy resonances are investigated with widths ranging from 0.1 to several GeV and Higgs masses varying in the range of 150 GeV to 850 GeV. No excess over the SM background has been found, and thus 95% C.L. upper bounds have been set on the production cross section times branching ratio in the above-mentioned Higgs mass range. In Fig. 7(a), we show the distribution of the quantity $\sigma \times \text{Br}(H \rightarrow \gamma\gamma)$ for all the points of our scanned data set (i.e., 2σ allowed points obtained after the global analysis with various Higgs signal strengths and flavour data, see Sec. 2). We then superimpose the bounds set by the CMS collaboration for two different choices of the Higgs decay width. The red solid line in Fig. 7(a) represents the case where Higgs decay width is 10% of the Higgs boson mass, while the blue dashed line represents the same but with fixed value of the Higgs decay width $\Gamma = 0.1 \text{ GeV}$. From the figure, one can see that all the points of our scanned data set satisfy the CMS bounds. A further investigation reveals that the Higgs to $\gamma\gamma$ branching ratio for all the points corresponding to the scanned dataset varies between $10^{-6} - 10^{-7}$ for all the points, and thus makes the quantity $\sigma \times \text{Br}(H \rightarrow \gamma\gamma)$ small enough to evade the CMS bound.

3.1.2 Search for H with WW final states

In the SM, the decay of Higgs boson to electro-weak gauge bosons (W/Z) provides interesting signatures at the LHC. In fact, the ZZ mode has a very good sensitivity to precisely measure the Higgs boson mass and its spin and parity [16, 17]. The CMS collaboration has searched for a SM-like Higgs boson decaying to a pair of W bosons with $(5 + 19.3) \text{ fb}^{-1}$ data collected at $\sqrt{s} = (7 + 8) \text{ TeV}$ at the LHC [59]. Analyzing the data with lepton, jets plus missing transverse energy final state signature, CMS collaboration excludes SM-like Higgs bosons in the mass ranges 170-180 GeV and 230-545 GeV at 95% C.L.. One can translate the bounds on the cross sections obtained from search of SM-like Higgs boson via this channel to the same corresponding to a model with additional Higgses. We calculate the product of production cross section and WW branching ratio, $\sigma \times \text{Br}(H \rightarrow WW)$, for our scanned points and then compare our findings with the CMS data. Note that we do not combine the 7 and 8 TeV data of LHC, rather we consider the exclusion limits of the 8 TeV data only. In Fig. 7(b), we superimpose the CMS exclusion limit on the 2σ allowed points obtained from global fit analysis. We find that updated CMS bound on production cross section with Higgs decaying to pair of W s is not sensitive enough to exclude the scanned parameter space. As we have already discussed, for almost all the points we are near the alignment limit (i.e. $(\beta - \alpha) \sim \frac{\pi}{2}$), which results into highly suppressed branching ratio of Higgs to the WW mode, $\text{Br}(H \rightarrow WW) \sim 10^{-2} - 10^{-4}$. This is the reason why the quantity $\sigma \times \text{Br}(H \rightarrow WW)$ is very small, and thus become insensitive to the CMS bound. We also find that even if we consider the (7+8) TeV combined CMS exclusion limit the parameter space will still remain allowed by the LHC data.

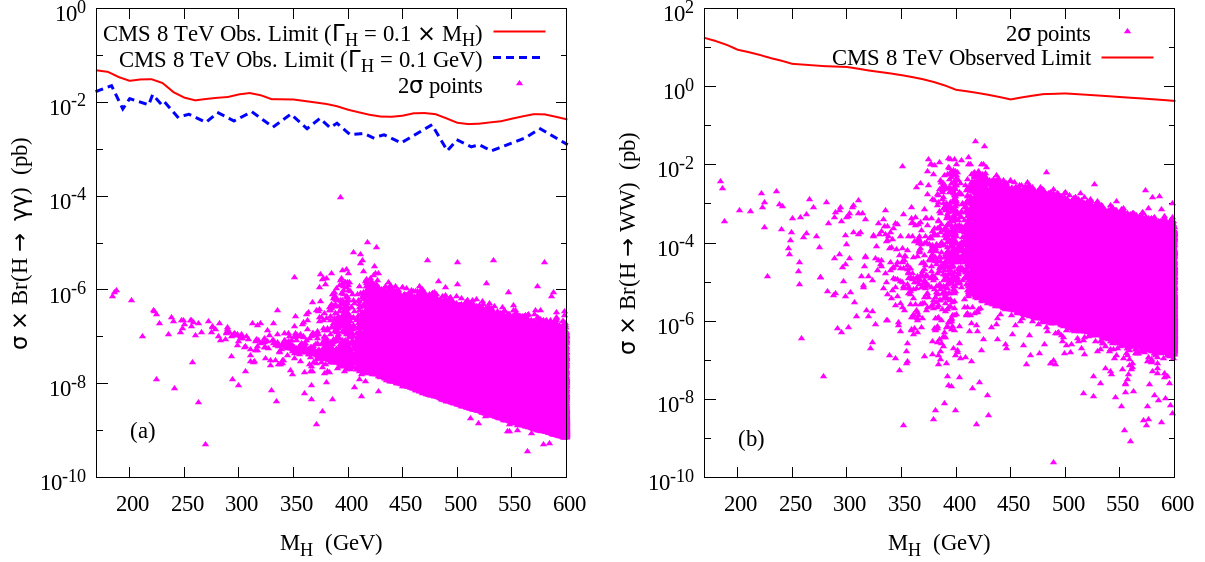


Figure 7: (a) Left: Scatter plot in $M_H - [\sigma \times \text{Br}(H \rightarrow \gamma\gamma)]$ plane assuming gluon-gluon fusion production process. The solid red (blue dashed) line represents the observed upper limits on $\sigma \times \text{Br}(H \rightarrow \gamma\gamma)$ at 95% C.L. by the CMS collaboration [56] using LHC-8 data with $\Gamma_H = 0.1 \times M_H$ (0.1 GeV). Magenta coloured triangle shaped points represent 2σ allowed parameter space from global fits satisfying flavour constraints (see Fig 1). (b) Right: Scatter plot in $M_H - [\sigma \times \text{Br}(H \rightarrow WW)]$ plane when the H is produced via ggF . The red solid line indicates the observed upper limits on $\sigma \times \text{Br}(H \rightarrow WW)$ at the 95% C.L. by the CMS collaboration [59] using LHC-8 data.

3.1.3 Search for H with hh ($b\bar{b}b\bar{b}$ and $b\bar{b}\gamma\gamma$) final states

The Higgs pair production cross section in the SM is very small, around 10 fb at $\sqrt{s} = 8$ TeV [57]. However, well-motivated BSM physics models predict the decay of narrow-width heavy resonances to a pair of 125 GeV Higgses, and thus one can expect enhancement in the 125 GeV Higgs pair production cross section. Search for these heavy resonances decaying to a pair of h , i.e. $pp \rightarrow X \rightarrow hh$ with X being the new heavy resonance, is performed by the CMS collaboration in the mass range of 260 - 1100 GeV with 19.7 fb^{-1} of data at $\sqrt{s} = 8$ TeV [57, 58]. The final state signatures that have been investigated by the CMS collaboration are: (i) $b\bar{b}b\bar{b}$ where both the Higgses decaying to $b\bar{b}$, and (ii) $b\bar{b}\gamma\gamma$ where one of the Higgs decays to $b\bar{b}$ while other decays to a pair of photons. The reconstruction of heavy resonance is possible in both the above-mentioned signatures, however $4b$ final state is experimentally challenging while $b\bar{b}\gamma\gamma$ channel has less background contamination and very good di-photon mass resolution. The observations by the CMS collaboration are consistent with the SM, and so 95% exclusion limits on the production cross sections are placed for the

entire mass range of the heavy resonance. At the LHC, the MSSM heavy CP even Higgs (H) can be generously produced from the ggF process, which then decays to a pair of 125 GeV Higgses. So, the bounds on the production cross section of new heavy resonances can be directly used to probe/exclude certain mass range of the heavy Higgs boson. To do so, we calculate the quantities $\sigma(pp \rightarrow H) \times \text{Br}(H \rightarrow hh \rightarrow b\bar{b}b\bar{b})$ and $\sigma(pp \rightarrow H) \times \text{Br}(H \rightarrow hh \rightarrow b\bar{b}\gamma\gamma)$ for all our scanned data set and in Fig. 8(a) and Fig. 8(b), we show the distributions of those two quantities respectively. The 95% C.L. upper limits (solid red line) imposed by the CMS collaboration on the respective distributions are also superimposed.

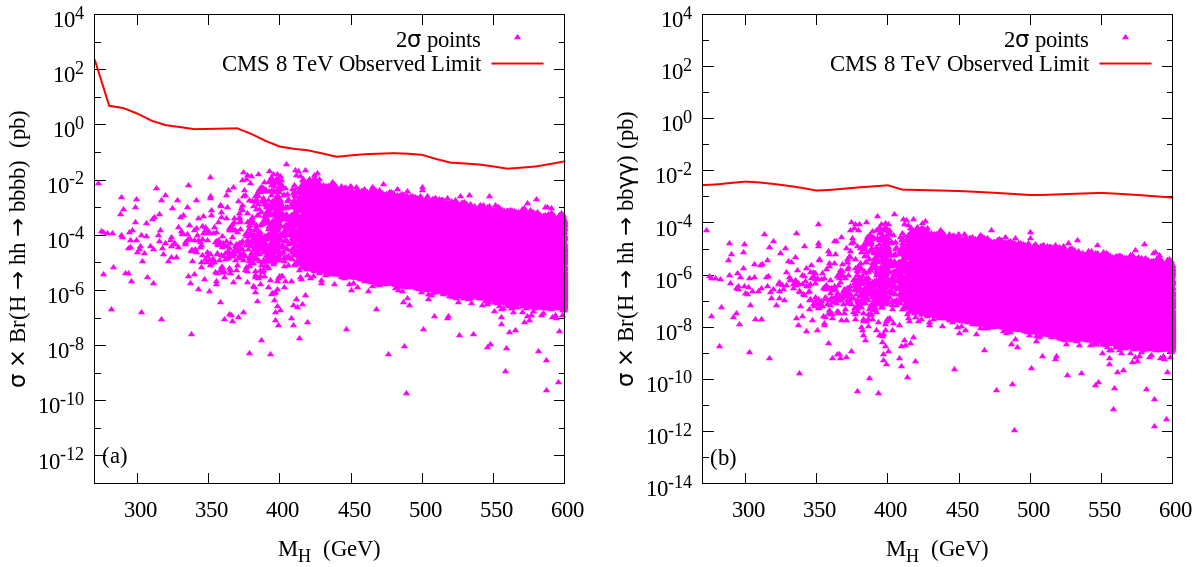


Figure 8: (a) Left: Scatter plot in $M_H - [\sigma \times \text{Br}(H \rightarrow hh \rightarrow b\bar{b}b\bar{b})]$ plane assuming gluon-gluon fusion production process for 2 σ allowed parameter space (represented by magenta points). The solid red line represents the observed upper limits on $\sigma \times \text{Br}(H \rightarrow hh \rightarrow b\bar{b}b\bar{b})$ at 95% C.L. by the CMS collaboration [58] using 8 TeV data. (b) Right: Scatter plot in $M_H - [\sigma \times \text{Br}(H \rightarrow hh \rightarrow b\bar{b}\gamma\gamma)]$ for ggF production mode. The red solid line indicates the observed upper limits on $\sigma \times \text{Br}(H \rightarrow hh \rightarrow b\bar{b}\gamma\gamma)$ at the 95% C.L. by the CMS collaboration [57] using LHC 8 TeV data.

The branching fraction of the MSSM heavy Higgs H to hh becomes sizable only for small $\tan \beta$ (≤ 5) and low M_A [20]. Once M_A becomes ≥ 350 GeV, the $t\bar{t}$ decay mode opens up and dominates in the rest of the parameter space. We find that so far CMS data can not exclude our 2 σ allowed parameter space, however the regions close to CMS exclusion lines corresponds to smaller values of $\tan \beta$, and so with one/two orders of improved measurement of di-Higgs production cross section at the Run-II of LHC, one can probe/exclude such regions of the parameter space. The ATLAS

collaboration has also searched for the heavy resonances (Kaluza-Klein excitation mode graviton) decaying to a pair of SM Higgses with both the Higgs decaying to a pair of b-quarks in the context of the Randall-Sundrum model [87]. The 95% exclusion limits set by the ATLAS collaboration are sensitive for heavy resonances (mass > 500 GeV) only, and thus is not directly applicable to the parameter space of interest, so we do not consider them in our analysis.

3.1.4 Search for H/A with $\tau^+\tau^-$ final states

The coupling of the MSSM heavy Higgs (H) and pseudoscalar Higgs (A) with down type fermion f_d (say bottom quark, tau lepton) is proportional to $\cos\alpha/\cos\beta$ and $\tan\beta$ respectively. So, for a fixed value of Higgs mixing angle α , both the couplings $Hf_d\bar{f}_d$ and $Af_d\bar{f}_d$ increases with $\tan\beta$. Thus for large values of $\tan\beta$ (say ≥ 10), both H and A dominantly decays to $b\bar{b}$ ($\sim 90\%$) and $\tau^+\tau^-$ ($\sim 10\%$), resulting into strong suppression in all other decay modes [20]. The production of the MSSM heavy Higgses is also primarily controlled by $\tan\beta$. The Higgses are dominantly produced via gluon-gluon fusion process and associated production with b-quarks i.e., $b\bar{b}\Phi$ ($\Phi=H,A$). All other production processes like VBF, associated production with gauge bosons, associated production with top quarks are dominantly suppressed for the heavy Higgses H/A due to small HVV/AVV and $Ht\bar{t}/At\bar{t}$ couplings [20]. The ATLAS and CMS collaborations at the LHC have studied the signatures of these heavy Higgses (H/A) produced via ggF and b-quark associated production processes, and decays to pair of τ -leptons [54, 55]. No excesses are observed over the SM backgrounds, and thus model independent bounds are placed on the production cross section times branching ratio $\sigma \times \text{Br}(\Phi \rightarrow \tau^+\tau^-)$ for different values of M_Φ with $\Phi = H/A$. In Fig. 9(a) and Fig. 9(b), we display our scanned points along with the upper limit on production cross section by the ATLAS and CMS collaborations for two dominant production modes, left panel corresponds to the ggF process while right panel represents the associated production process $b\bar{b}\Phi$, $\Phi = H, A$. In order to compare our findings with the ATLAS [54] and CMS [55] data, in Fig. 9(a) and Fig. 9(b) we show the distributions of $\sigma \times \text{Br}(\Phi \rightarrow \tau^+\tau^-)$ combining the contributions of both H and A for the two different production mechanism.

It is evident from Fig. 9 that the LHC data from the $H \rightarrow \tau^+\tau^-$ channel has significant impact on the 2σ allowed parameter space. In fact, the entire region with $\tan\beta > 20$ and significant amount of parameter space with $\tan\beta > 10$ are excluded when the Higgs is produced via $b\bar{b}\Phi$ process. However, sensitivity of this channel with ggF production process is negligible. For a better understanding of the sensitivity of $\tau^+\tau^-$ channel, we display the scanned dataset with explicit $\tan\beta$ dependence, regions with $30 < \tan\beta < 50$, $20 < \tan\beta < 30$, $10 < \tan\beta < 20$ and $1 < \tan\beta < 10$ are shown in pink (cross), green (triangle), blue (circle) and violet (square) respectively. One can now clearly see that the regions with large $\tan\beta$ implies large coupling with b and τ s and so large $\sigma \times \text{Br}$, and thus more stringent constraint by the LHC data.

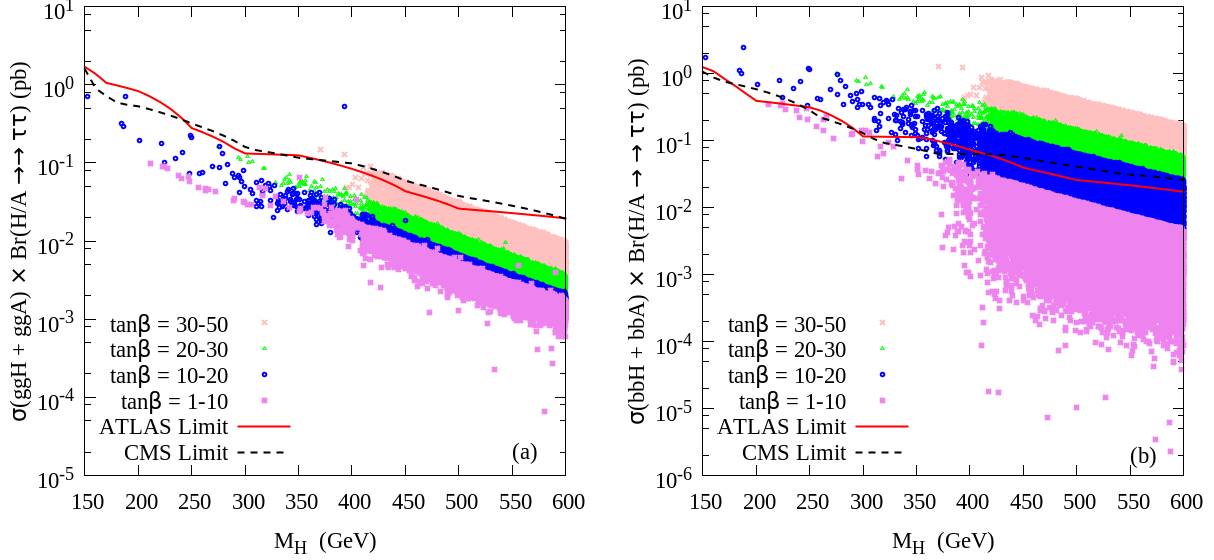


Figure 9: Scatter plot in $M_H - [\sigma \times \text{Br}(\Phi \rightarrow \tau^+\tau^-)]$ plane where $\Phi = H, A$ produced via (a) gluon fusion and (b) in association with b -quarks. The solid red (black dashed) line represents the observed upper limits on $\sigma \times \text{Br}(\Phi \rightarrow \tau^+\tau^-)$ at 95% C.L. by the ATLAS (CMS) collaboration using LHC-8 data [54, 55]. Combined contributions of $\sigma \times \text{Br}(\Phi \rightarrow \tau^+\tau^-)$ of both H and A for the 2σ allowed parameter space with $30 < \tan\beta < 50$, $20 < \tan\beta < 30$, $10 < \tan\beta < 20$ and $1 < \tan\beta < 10$ are shown in pink (cross), green (triangle), blue (circle) and violet (square) respectively.

3.1.5 Search for A with Zh final states

Similar to the case where we discussed the possibility of heavy resonances decaying to a pair of MSSM lightest Higgs bosons (see Sec. 3.1.3), one can also consider the possibility of having h in association with Z boson from the decay of pseudoscalar Higgs boson A when M_A is greater than $(M_h + M_Z)$. However, the decay rate $\Gamma(A \rightarrow Zh)$ is appreciable only at very low values of $\tan\beta$ (< 10) and for M_A below the $t\bar{t}$ threshold i.e., approx. 350 GeV. Once the $t\bar{t}$ decay opens up, it dominates for all values $M_A > 350$ GeV and $\tan\beta < 10$ [20]. The CMS collaboration at the LHC has searched for the heavy pseudoscalar Higgs bosons when it decay to a Z boson and a light Higgs boson (h). The final state includes two opposite sign leptons (from Z decay) and two b -quarks (from h decay). Thus, one can fully reconstruct the mass of A using the four momentum information of the final state leptons and b -jets. In fact three clear distinguishable resonance peaks, at M_Z , M_h and M_A , are expected for the signal events. Both the ATLAS and CMS collaborations have performed the search for the heavy pseudoscalar Higgs bosons at the 8 TeV run of LHC [60, 61]. No significant excesses over SM background are observed in the ATLAS

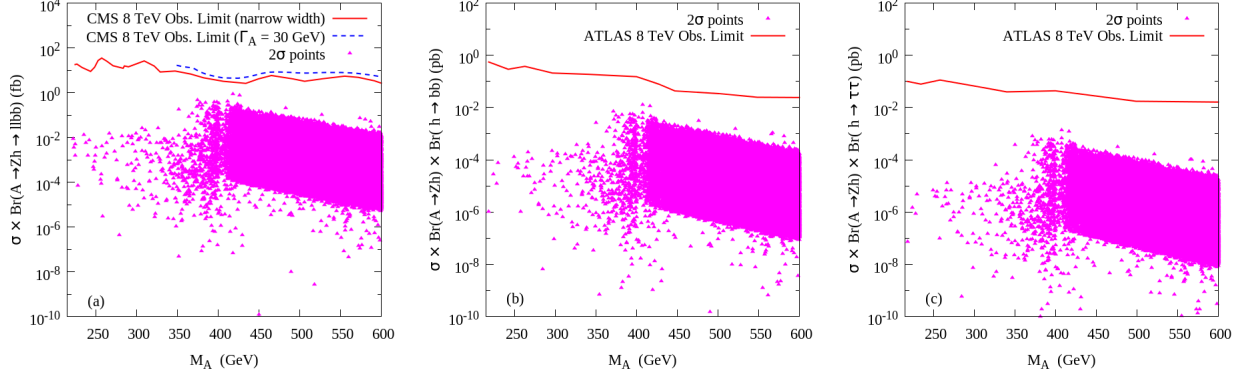


Figure 10: (a) Left: Scatter plot in $M_A - [\sigma \times \text{Br}(A \rightarrow Zh \rightarrow \ell^+ \ell^- b\bar{b})]$ plane assuming gluon-gluon fusion production process for 2σ allowed parameter space (represented by magenta points). The solid red (blue dashed) line represents the observed upper limits on $\sigma \times \text{Br}(A \rightarrow Zh \rightarrow \ell^+ \ell^- b\bar{b})$ at 95% C.L. by the CMS collaboration using LHC-8 data [61] with narrow width ($\Gamma_A = 30$ GeV) assumption. (b) Middle: Scatter plot in $M_A - [\sigma \times \text{Br}(A \rightarrow Zh) \times \text{Br}(h \rightarrow b\bar{b})]$ plane for ggF production mode. The red solid line indicates the observed upper limits on $\sigma \times \text{Br}(A \rightarrow Zh) \times \text{Br}(h \rightarrow b\bar{b})$ at the 95% C.L. by the ATLAS collaboration using LHC 8 TeV data [60]. (c) Right: Scatter plot in $M_A - [\sigma \times \text{Br}(A \rightarrow Zh) \times \text{Br}(h \rightarrow \tau^+ \tau^-)]$ plane for ggF production mode. The red solid line shows the observed upper limits on $\sigma \times \text{Br}(A \rightarrow Zh) \times \text{Br}(h \rightarrow \tau^+ \tau^-)$ at the 95% C.L. by the ATLAS collaboration using LHC 8 TeV data [60].

and CMS data. Thus model independent 95% C.L. upper limits are imposed on the production cross section of A times $\text{Br}(A \rightarrow Zh)$. In Fig. 10(a) and (b), we present the 2σ allowed scanned data points along with the CMS and ATLAS exclusion limits respectively. The solid red exclusion line in Fig. 10(a) assume narrow-width resonance, while the blue dashed line consider the 30 GeV decay width of A boson. The ATLAS collaboration has also performed their study with narrow width approximation, however they have analyzed two possible decay modes of the Higgs boson, namely $b\bar{b}$ and $\tau^+ \tau^-$. In Fig. 10(b) we display the allowed parameter space with $b\bar{b}$ final state, while Fig. 10(c) shows the same but with $\tau^+ \tau^-$ final state. As we already mentioned, this decay mode plays an important role only in the region with small $\tan \beta$ and low M_A . We find that in the parameter space of our interest, ATLAS and CMS data are not sensitive enough to impose any additional constraints. We expect these heavy pseudoscalar Higgses will be probed with improved measurement of these decay modes in the run-II of LHC.

3.2 Charged Higgs boson searches

3.2.1 Search for H^\pm with $\tau\nu$ and $c\bar{s}$ final states

The SM particle content does not include a charged scalar particle, however models with additional Higgs doublets predict charged Higgs bosons (H^\pm). Thus the discovery of a charged scalar particle is a clear signature of the BSM physics. The large electron positron collider (LEP) searched for the charged Higgs bosons with center-of-mass energy $\sqrt{s} = 209$ GeV. LEP did not find any signal of charged Higgs boson which then leads to put bounds on mass of the charged Higgs boson $M_{H^\pm} > 78.6$ GeV [88]. The production and decay of H^\pm primarily depend on M_{H^\pm} and top quark mass, more precisely on whether $M_{H^\pm} < M_{\text{top}}$ or $M_{H^\pm} > M_{\text{top}}$. If the charged Higgs boson is lighter than the top quark, i.e., $M_{H^\pm} < (m_t - m_b)$, then H^\pm is mostly produced from the $t\bar{t}$ process. The decay of H^\pm depends on the coupling of the charged Higgs boson with the fermions which is mainly controlled by $\tan\beta$. The coupling is large for very low and very large values of $\tan\beta$ and small for intermediate values. Thus, for light enough H^\pm it is primarily produced from the $t\bar{t}$ process and dominantly decays into $\tau\nu_\tau$ final states. It is to be noted that light charged Higgs bosons ($M_{H^\pm} < M_t$) can also decay to a charm and a anti-strange quark, and thus in certain regions of parameter space one can expect some competition between the $c\bar{s}$ and $\tau\nu_\tau$ decay modes. Now, if the H^\pm is heavy i.e., $M_{H^\pm} > M_{\text{top}}$, then they are mainly produced in associated production with a top quark i.e., $pp \rightarrow tH^\pm + X$. For small $\tan\beta$, H^\pm exclusively decays to a top and bottom quark, however for large values of $\tan\beta$ the decay of H^\pm to $\tau\nu_\tau$ is not negligible i.e., $\text{Br}(H^\pm \rightarrow \tau^\pm\nu_\tau) \sim 10\%$ [20].

Both CMS and ATLAS collaborations have searched for the charged Higgs bosons at the 8 TeV run of LHC using the top-quark pair production process and associated production of H^\pm with a top quark. Search for the light charged Higgs bosons decaying to a τ and a tau-neutrino (ν_τ), and/or to a charm and strange quark are also presented by the ATLAS and CMS collaborations [62–65]. The results seem to agree with the SM predictions and non observation of the excesses leads to 95% C.L. exclusion limits on the production cross section times branching ratios for different values of M_{H^\pm} .

Now, we find that all the points of the scanned data set corresponds to $M_{H^\pm} > 200$ GeV and thereby the decay $t \rightarrow bH^\pm$ is kinematically forbidden, and so ATLAS and CMS bounds on M_{H^\pm} using the $t\bar{t}$ sample have no effect on the parameter space of interest. However, we do impose the ATLAS and CMS bounds on M_{H^\pm} considering the production of charged Higgs boson in association to a top and bottom quark with H^\pm decaying to $\tau^\pm\nu_\tau$. In Fig.11(a), we superimpose the ATLAS and CMS bounds on the points corresponding to our data set. We check that the bounds using the $c\bar{s}$ mode are not applicable. From Fig.11(a) one can infer that one/two orders of improvement in cross section measurement might help to probe the parameter space of interest.

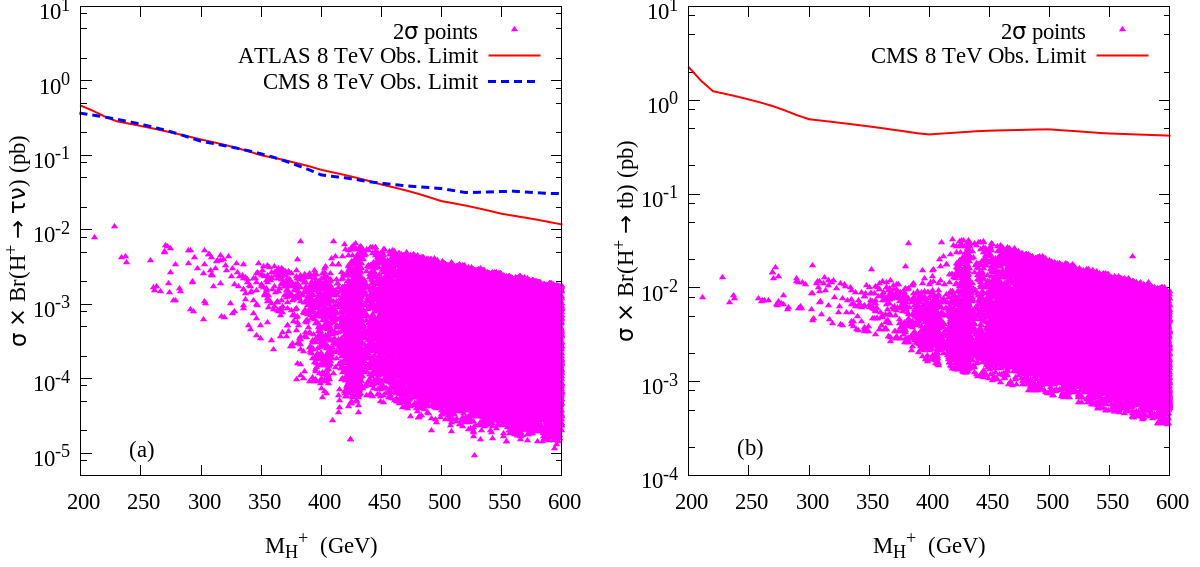


Figure 11: (a) Left: Scatter plot in $M_{H^\pm} - [\sigma \times \text{Br}(H^\pm \rightarrow \tau^\pm \nu_\tau)]$ plane for ggF production. Magenta points represent 2σ allowed regions. The solid red (blue dashed) line represents the observed upper limits on $\sigma \times \text{Br}(H^\pm \rightarrow \tau^\pm \nu_\tau)$ at 95% C.L. by the ATLAS [62] (CMS) collaboration using LHC 8 TeV data. (b) Right: Scatter plot in $M_{H^\pm} - [\sigma \times \text{Br}(H^\pm \rightarrow t\bar{b})]$ plane for ggF production. The solid red line shows the observed upper limits on $\sigma \times \text{Br}(H^\pm \rightarrow t\bar{b})$ at 95% C.L. by the CMS collaboration using LHC 8 TeV data.

3.2.2 Search for H^\pm with $t\bar{b}$ final states

As we have already mentioned, the decay of H^\pm to a top and bottom quark dominates in the regions with $M_{H^\pm} > M_{top}$. They are primarily produced via $gg \rightarrow tbH^\pm$ process. However processes like $q\bar{q} \rightarrow H^+H^-$, associated production with neutral Higgses can give small contributions to the dominant tbH^\pm process. The decay of H^\pm is completely controlled by the single parameter $\tan\beta$. For small values of $\tan\beta$ it is the dominant decay mode (branching ratio is close to unity), however at high $\tan\beta$ the branching ratio decreases slightly $\text{Br}(H^\pm \rightarrow t\bar{b}) \sim 90\%$ while $\text{Br}(H^\pm \rightarrow \tau^\pm \nu_\tau) \sim 10\%$. The CMS collaboration have searched for the charged Higgs bosons with H^\pm decaying to a top and bottom quark [66]. The process under consideration looks like $gg \rightarrow H^\pm tb \rightarrow (\ell \nu_\ell b\bar{b})(\ell' \nu_{\ell'} b)$, with ℓ, ℓ' being an electron or a muon. The search is performed with 19.7 fb^{-1} of data at $\sqrt{s} = 8$ TeV. No evidence for a charged Higgs signal is found and thus upper limits on the production rates are placed for H^\pm masses in the range of 180-600 GeV. We calculate the $gg \rightarrow tbH^\pm$ production cross section for all our valid points, and then impose the CMS bounds. We present our results in Fig. 11(b), where the solid red line indicates the CMS exclusion limit. It is evident from the figure

that $t\bar{b}$ mode is not sensitive enough to put any strong bound on the parameter space.

4 SUSY Higgs : Future limits

4.1 Heavy Higgs search

In the last section, we discussed the limits on the allowed parameter space of the MSSM Higgs sector coming from the direct searches at LHC run-I. We show that significant amount of parameter space with additional light Higgses are still allowed by the LHC data. Additionally, we also found that the production of heavy Higgs bosons in association with the bottom quarks with H/A decaying to $\tau^+\tau^-$ provides the most stringent bound on our parameter space and the regions with large values of $\tan\beta$ (> 20) are excluded by the $\tau^+\tau^-$ decay mode. In this section, we discuss the sensitivity of HL-LHC for the heavy Higgses through the following decay modes: $H \rightarrow hh$, $H \rightarrow t\bar{t}$, $A \rightarrow Zh$ and $H/A \rightarrow \tau^+\tau^-$. Note that, these channels⁴ are expected to be most sensitive at the regions with $\tan\beta < 20$. Additionally, we also consider the decay $H \rightarrow ZZ$ following the ATLAS and CMS analysis [94,95] at 14 TeV run of LHC with 3000 fb^{-1} of integrated luminosity.

4.1.1 Search for H with 4ℓ final states

Both the ATLAS and CMS collaborations have looked for the heavy Higgs bosons which are produced via ggF process and decayed into ZZ ($Z \rightarrow \ell\ell$, $\ell = e, \mu$) at 14 TeV HL-LHC [94,95]. In their analyses, the ATLAS collaboration has considered the decay width of H to be the same as that of a SM-like Higgs boson for a given mass, while the CMS collaboration calculated the width of H assuming $\tan\beta = 1$ and $\cos(\beta - \alpha) = -0.06$. The expected 95% C.L. exclusion limits on $\sigma \times \text{Br}(H \rightarrow ZZ \rightarrow 4\ell)$ at $\mathcal{L} = 3000 \text{ fb}^{-1}$ by the ATLAS and CMS collaborations are quite similar as shown in Fig. 12 by red solid and blue dashed line respectively. We calculate the quantity $\sigma \times \text{Br}(H \rightarrow ZZ \rightarrow 4\ell)$ for all the points in our scanned data set and then compare our results with ATLAS and CMS predictions [94,95]. In Fig. 12 we overlay the experimental predictions with our scanned data set shown in magenta triangles. We find that for most of the parameter space points, even for the points with large production cross sections, the branching ratio $\text{Br}(H \rightarrow ZZ)$ is very small ($\sim 10^{-3}$ to 10^{-5})⁵, which results into smaller values of $\sigma \times \text{Br}(H \rightarrow ZZ \rightarrow 4\ell)$. We thus find that most of the parameter space points are beyond the reach of HL-LHC for $H \rightarrow 4\ell$ final state.

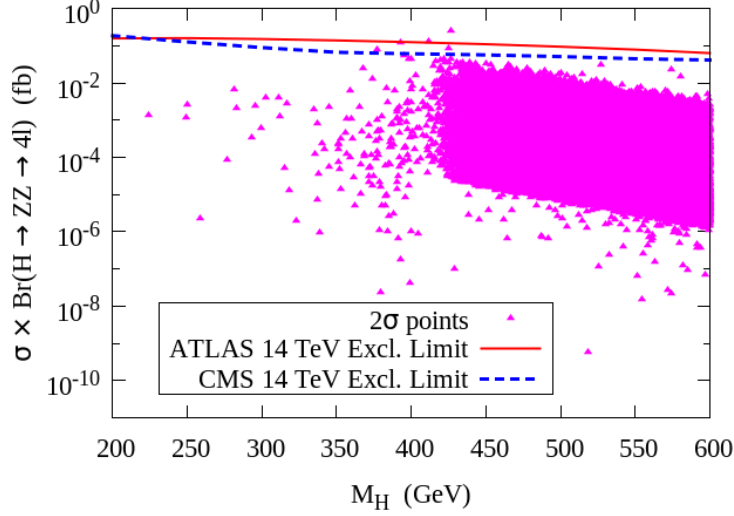


Figure 12: Scatter plot in $M_H - [\sigma \times \text{Br}(H \rightarrow ZZ \rightarrow \ell^+ \ell^- \ell^+ \ell^-)]$ plane assuming gluon-gluon fusion production process. Magenta colored points represents for 2σ allowed parameter space. The solid red line (blue dashed line) represents the expected upper limits on $\sigma \times \text{Br}(H \rightarrow ZZ \rightarrow \ell^+ \ell^- \ell^+ \ell^-)$ at 95% C.L. by the ATLAS (CMS) collaboration [94, 95] for 14 TeV LHC with $\mathcal{L} = 3000 \text{ fb}^{-1}$.

4.1.2 Search for pseudoscalar A with $\ell^+ \ell^- b\bar{b}$ final states

In the regions below the $t\bar{t}$ threshold and small $\tan\beta$ the pseudoscalar Higgs A decays to Zh with an appreciable amount. An interesting feature of this decay mode with $Z \rightarrow \ell^+ \ell^-$ and $h \rightarrow b\bar{b}$ is that one can fully reconstruct the mass A using the four momentum of the leptons and b-jets. ATLAS and CMS collaborations have analysed the sensitivity of this channel at the HL-LHC via ggF process [94, 95]. In order to present the expected 95% C.L. exclusion limits ATLAS has assumed a narrow width approximation (i.e., width of A is much smaller than the experimental resolution) while CMS has calculated the width of A by assuming $\tan\beta = 1$ and $\cos(\beta - \alpha) = -0.06$. In Fig. 13, we show the distribution of $\sigma \times \text{Br}(\rightarrow Zh \rightarrow \ell\ell b\bar{b})$ for all the points in the scanned data set, and then overlay the 95 % C.L. upper limits by the ATLAS (red solid line) and CMS (blue dashed line) collaborations [94, 95] at 14 TeV LHC with $\mathcal{L} = 3000 \text{ fb}^{-1}$. We find that the ATLAS limits are more stronger (by almost one order) than the CMS, although the reason behind this is apparently not clear. From the Fig. 13 it is clear that only a very small region of the parameter space will be excluded by the HL-LHC data, in fact to probe the remaining parameter space few

⁴Reach of heavy Higgs bosons have been discussed in the literature in the context of 8/14 TeV run of LHC, for details see Refs. [89–93].

⁵ The result is consistent with the alignment limit.

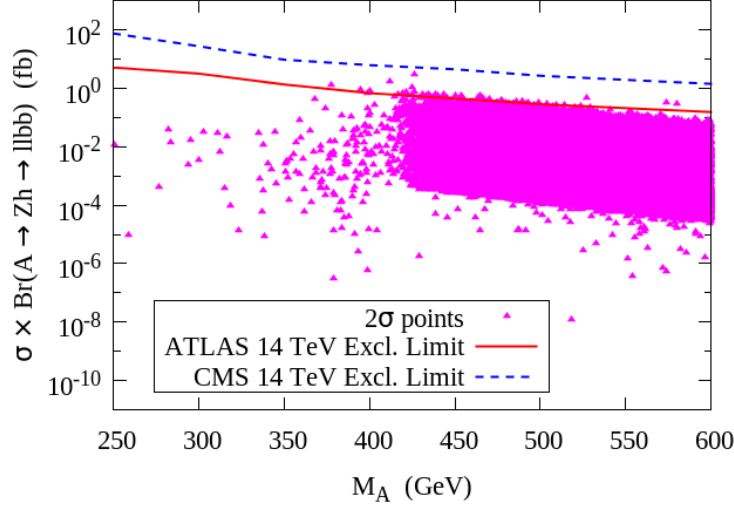


Figure 13: Scatter plot in $M_A - [\sigma \times \text{Br}(A \rightarrow Zh \rightarrow \ell^+ \ell^- b \bar{b})]$ plane assuming gluon-gluon fusion production process. Magenta colored points represents for 2σ allowed parameter space. The solid red line (blue dashed line) represents the expected upper limits on $\sigma \times \text{Br}(A \rightarrow Zh \rightarrow \ell^+ \ell^- b \bar{b})$ at 95% C.L. by the ATLAS (CMS) collaboration for 14 TeV LHC with $\mathcal{L} = 3000 \text{ fb}^{-1}$ [94, 95].

orders of magnitude improvement in cross section measurement is required.

4.1.3 Search for H with di-higgs ($H \rightarrow hh \rightarrow b\bar{b}\gamma\gamma$) final states

In this subsection we discuss the possibility of observing the heavy CP even Higgs boson (H) at HL-LHC with its decay to a pair of SM-like Higgses (h) with one Higgs decaying to $b\bar{b}$ and other to $\gamma\gamma$ modes. Single H production cross section can be up to two orders of magnitude larger compared to the direct h pair production cross section (see Table 1 of Ref. [96])⁶ depending on the choice of model parameters and it can also have non-trivial effects on the self coupling measurement of the 125 GeV Higgs [96].

In the MSSM, the production cross section of H and its decay to a pair of SM-like Higgses crucially depends on the SUSY parameter space, mainly M_A and $\tan\beta$. More precisely, below the $t\bar{t}$ threshold (350 GeV), the decay rate $\Gamma(H \rightarrow hh)$ is substantial only for smaller values of $\tan\beta$. The most dominant production mechanism of H is the ggF process although, for large or moderate $\tan\beta$, the bottom quark annihilation to H ($b\bar{b} \rightarrow H$) cross section can be substantial [97]. The final state signature, depending on the decay of the SM-like Higgses, includes, for example, $b\bar{b}b\bar{b}$,

⁶The SM Higgs pair production cross section at next to leading order is about 34 fb at 14 TeV LHC for $M_h = 125$ GeV [98].

$b\bar{b}\tau^+\tau^-$, $b\bar{b}W^+W^-$, $b\bar{b}\gamma\gamma$ etc. Among all these possibilities, $b\bar{b}b\bar{b}$ final state has the largest cross section. However, due to enormous QCD background this is one of the most challenging scenarios to be observed at the LHC⁷. On the other hand, even though the branching ratio for $b\bar{b}\gamma\gamma$ channel is very small (about 0.27 %), it is the most promising channel due to large photon identification efficiency and very good resolution in the photon energy measurement. Hence using the di-photon invariant mass distribution one can easily reconstruct the Higgs boson mass and at the same time separate the signal from the SM background⁸.

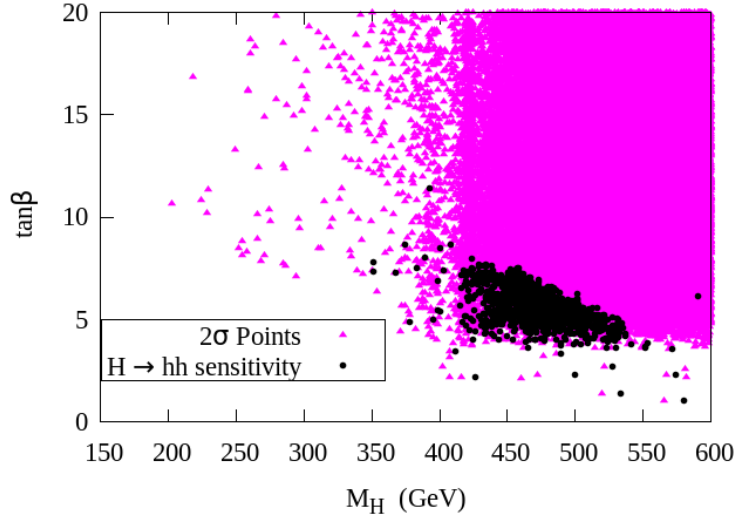


Figure 14: *Sensitivity of di-Higgs final state in $M_A - \tan\beta$ plane at HL-LHC from $b\bar{b}\gamma\gamma$ channel with $\mathcal{L} = 3000 \text{ fb}^{-1}$. The magenta coloured points are 2σ allowed points from global analysis and the black circled points are expected to be probed at HL-LHC (see Sec.4.1.3 for details).*

A detailed signal-background analysis of heavy Higgs production and its decay to a pair of 125 GeV Higgs in $b\bar{b}\gamma\gamma$ channel has been already performed in Ref. [96]. Here we use their results to constrain our parameter space⁹. Events with two b -jets, two photons and no isolated leptons are selected after imposing the basic selection cuts following the ATLAS collaboration [101]. Using the four momentum information of the $b\bar{b}$ and $\gamma\gamma$ system, the invariant mass of the heavy Higgs boson can be reconstructed assuming $M_{b\bar{b}\gamma\gamma}$ is $M_H \pm 50 \text{ GeV}$.

⁷ It has been shown that the jet substructure technique can be very useful to separate the signal events from the large QCD and electroweak backgrounds [99].

⁸In this case, the dominant backgrounds are $t\bar{t}h$ and the direct Higgs pair production (hh). Note that, the production cross section for both the Higgs pair and $t\bar{t}h$ processes depend on the MSSM parameters, however, here we assume SM cross sections for hh and $t\bar{t}h$ processes.

⁹The analysis for $b\bar{b}\gamma\gamma$ channel was first introduced in the Ref. [100]

Let us now estimate the sensitivity of the HL-LHC to probe the parameter space in the $b\bar{b}\gamma\gamma$ channel. In Ref. [96], authors considered few representative benchmark points with heavy Higgs mass M_H in the range of 275 - 600 GeV and performed a detailed collider analysis. We should note, as also pointed out in Ref. [96], the cut efficiencies do not change radically in the entire region of 275 - 600 GeV. The number of background events (N_B) and the cut efficiencies as a function of M_H are taken from Ref. [96]. We estimate the number of signal events (N_S) for all the points in the scanned data set by multiplying the cut efficiencies with the production cross sections, and then calculate the signal significance $\mathcal{S} = N_S/\sqrt{N_B}$. In Fig. 14, we present the sensitivity of the $b\bar{b}\gamma\gamma$ channel at HL-LHC where magenta triangles corresponds to our scanned data set, while the black circles represent the points with $\mathcal{S} > 2\sigma$. In other words, these are the points (black circle) with low $\tan\beta$ (< 10) that are expected to be probed at the HL-LHC. The lack of sensitivity of HL-LHC in the regions of parameter space with $\tan\beta > 10$ is due to the fact that both the ggF production cross section and $\text{Br}(H \rightarrow hh)$ decreases with the increase of $\tan\beta$ forcing this portion of parameter space to go beyond the reach of HL-LHC. From the Fig. 14, one can note that future run of LHC might not be able to exclude the entire region below $M_H \lesssim 425$ GeV and $\tan\beta \lesssim 8$.

4.1.4 Search for H/A with $t\bar{t}$ final state

Above the kinematic threshold of $t\bar{t}$ (~ 350 GeV), the decay of H and A into $t\bar{t}$ pair opens up. In fact, for $M_A > 350$ GeV and low to moderate values of $\tan\beta$, it is indeed the dominant decay mode of H/A . Besides, due to large top-Higgs Yukawa coupling, the production cross section of the heavy Higgs H via ggF process also becomes large in the low $\tan\beta$ regime. Hence, assuming the narrow width approximation, one can expect to observe a resonance peak at $M_{H/A}$ in the $t\bar{t}$ invariant mass distribution. However, the main drawback of such a bump hunting procedure is that it is extremely difficult to extract the $t\bar{t}$ resonance peak from the huge SM $t\bar{t}$ continuum background. Here, we perform a detailed signal-background analysis in the context of HL-LHC and study the sensitivity of HL-LHC to probe the region of parameter space of our interest.

We analyze the production of heavy Higgses H/A via ggF process and their decay to $t\bar{t}$ ¹⁰, where one top decays leptonically and one decays hadronically. So, the final state includes one isolated lepton (electron or muon), at least four jets among them at least two are b -jets and missing transverse energy (E_T). We use PYTHIA (version 6.4.28) [86] to generate both the signal and dominant SM background, e.g., $t\bar{t}$ events. Electrons are selected with $p_T > 20$ GeV and $|\eta| < 2.47$, while we choose muons with $p_T > 20$ GeV and $|\eta| < 2.4$. We select jets with $p_T > 30$ GeV and $|\eta| < 2.8$. A jet is called a “ b -jet” if the angular separation $\Delta R = \sqrt{(\Delta\eta)^2 + (\Delta\phi)^2}$ in the $\eta - \phi$ plane between the jet and a B -hadron is less than 0.2. Following the ATLAS collaboration, we also assume a flat 70% b -tagging efficiency for the b -jets [102]. In our analysis, we also implement

¹⁰As H and A are almost degenerate, one might not be able to distinguish them in $t\bar{t}$ invariant mass distribution. For this reason, here we consider the production of the heavy Higgses H/A simultaneously via the ggF process.

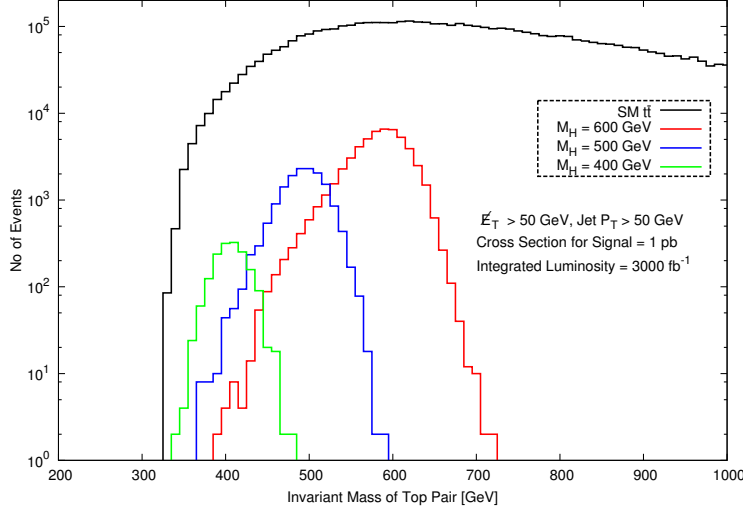


Figure 15: *Distribution of $t\bar{t}$ invariant mass for some representative SUSY benchmark points with $M_H = 400$ GeV (green), 500 GeV (blue), 600 GeV (red) and SM $t\bar{t}$ background (black). The distribution has been drawn before applying the cut on invariant mass (C5) in signal region SR-loose (see text for details) for integrated luminosity $\mathcal{L} = 3000 \text{ fb}^{-1}$. We consider NNLO+NNLL cross section for SM $t\bar{t}$ production at 14 TeV LHC (966 pb) and for signal the no of events has been estimated assuming single H production cross section to be 1 pb with $\text{Br}(H \rightarrow t\bar{t}) = 100\%$.*

the methodology of lepton isolation and lepton-jet identification following the ATLAS study [103]. Although it is possible to reconstruct leptonically decaying top quark within a quadratic ambiguity, for simplicity we use the parton level four momentum information of the neutrino to reconstruct the H mass.

We are now in a position to describe the details of our simulation procedure as well as the kinematic selection cuts for our signal and the backgrounds. We choose three representative benchmark points with $M_H = 400, 500$ and 600 GeV, and define three signal regions (SR), namely *SR-loose*, *SR-medium*, *SR-tight*, depending on the choice of our selection cuts. The SR-loose is defined based on the following set of cuts:

- C1: Events must contain at least 4 jets with $p_T > 50$ GeV.
- C2: Among the four selected jets, two are b -tagged.
- C3: Events containing one isolated lepton with $p_T > 30$ GeV are selected.
- C4: Missing energy (E_T) > 50 GeV.
- C5: Select events with $t\bar{t}$ invariant mass between $M_H \pm 25$ GeV.

We denote the signal region *SR-medium* with the same set of cuts as that of *SR-loose* but with $\cancel{E}_T > 100$ GeV. In order to probe higher values of M_H , we define the signal region *SR-tight* where the cuts on p_T of the jets and \cancel{E}_T are stronger. For example, for *SR-tight*, events are selected with p_T of the first two leading jets greater than 100 GeV while the missing transverse energy $\cancel{E}_T > 100$ GeV.

Channel	Number of Events at 3000 fb ⁻¹					
	$M_H = 400$ GeV		$M_H = 500$ GeV		$M_H = 600$ GeV	
	Signal	$t\bar{t}$	Signal	$t\bar{t}$	Signal	$t\bar{t}$
<i>SR-loose</i>	1268	104612	9658	420572	26842	563452
<i>SR-medium</i>	8	1741	1584	69232	9656	194698
<i>SR-tight</i>	-	-	4	637	2296	44894

Table 7: Number of signal (H production via ggF) and SM $t\bar{t}$ events after applying the cuts in *SR-Loose*, *SR-Medium* and *SR-Tight* signal region at 14 TeV LHC with $\mathcal{L} = 3000$ fb⁻¹. For $t\bar{t}$, we use NNLO cross section [104]. For the signal estimation we present the number assuming $\sigma(pp \rightarrow H)_{NLO} \times Br(H \rightarrow t\bar{t}) = 1$ pb.

In Fig. 15, we display the $t\bar{t}$ invariant mass distribution for the three representative benchmark points with $M_H = 400$ GeV (green), 500 GeV (blue), 600 GeV (red), and also overlay the same for the SM $t\bar{t}$ background (black line). We show the invariant mass distribution for the signal region *SR-loose* with an integrated $\mathcal{L} = 3000$ fb⁻¹. To estimate the number of background events, we use the $t\bar{t}$ cross section at next-to next-to leading order (NNLO) $\sigma_{NNLO}^{t\bar{t}} = 966$ pb [104]. For simplicity, we assume that for all the benchmark points $Br(H \rightarrow t\bar{t})$ is 100% and the next-to leading order production cross section $\sigma(pp \rightarrow H)$ is 1 pb. Note that, we make such a conservative choice just to keep our analysis simple, one can easily scale our numbers with the actual production cross sections and branching ratios. Although one can see clear resonance peaks at the M_H masses (see Fig. 15), enormous SM $t\bar{t}$ background makes it very challenging to observe a clear signal of heavy Higgs in the $t\bar{t}$ invariant mass distribution over the SM background. To be more precise, we count the number of signal and background events for three signal regions *SR-loose*, *SR-medium* and *SR-tight* after C5, and then calculate the statistical significance $\mathcal{S} = N_S/\sqrt{N_B}$. In Table 7, we present the number of signal and background events for three benchmark points and the SM $t\bar{t}$ backgrounds at the 14 TeV run of LHC with $\mathcal{L} = 3000$ fb⁻¹. From Table 7 one can see that N_S/N_B ratio is very small for all the benchmark points irrespective of the signal regions. We find that the statistical significances \mathcal{S} for $M_H = 600$ GeV are 36, 22 and 11 for the three signal regions *SR-loose*, *SR-medium* and *SR-tight* respectively. However, even with 5% systematic uncertainty these numbers reduces to 0.95, 0.99, 1.02 respectively.

In Fig. 16 we show the distribution of $\sigma \times Br(H, A \rightarrow t\bar{t})$ assuming production of both H and

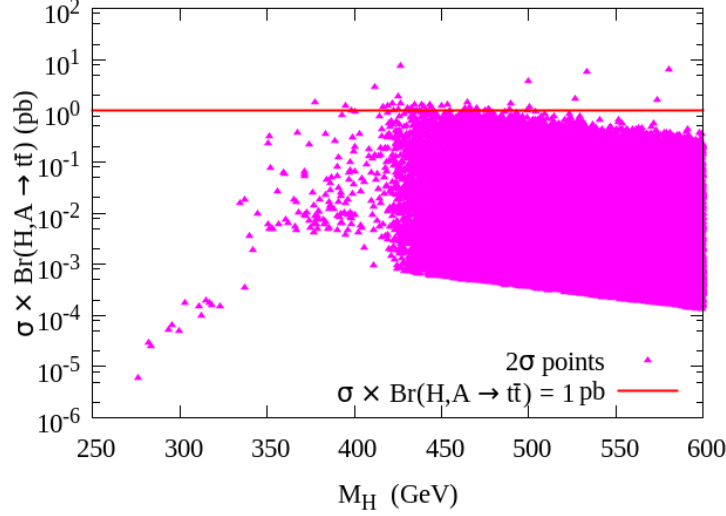


Figure 16: Scatter plot in $M_H - [\sigma \times \text{Br}(H, A \rightarrow t\bar{t})]$ plane assuming both H and A production via ggF at 14 TeV LHC. Magenta colored points represents for 2σ allowed parameter space. Red line corresponds to $\sigma \times \text{Br}(H, A \rightarrow t\bar{t}) = 1 \text{ pb}$.

A via ggF for all the points in our scanned data set. We find that $\sigma \times \text{Br}(H, A \rightarrow t\bar{t})$ lies mostly in the region 0.5 - 0.0001 pb. The red solid line in Fig. 16 represents $\sigma \times \text{Br}(H, A \rightarrow t\bar{t}) = 1 \text{ pb}$. This red solid line indicates that for most the points in our scanned data set the quantity cross section times $\text{Br}(H, A \rightarrow t\bar{t})$ is 10 - 1000 times smaller, and thus the the numbers in Table 7 represent a too much optimistic scenario. In other words, even HL-LHC might not be sensitive enough to probe such a region of parameter space.

Recently, it has been shown that using angular cuts, the signal significance can be improved [105]. However, one should note that the inclusion of systematic uncertainties may change the significance drastically and it is not possible to predict the reach of the $t\bar{t}$ channel at the HL-LHC without the precise knowledge of the systematic uncertainties. We end this section by mentioning that the observation of a heavy Higgs in $H \rightarrow t\bar{t}$ channel at the HL-LHC is really a challenging task and it needs special attention and more detailed studies.

4.1.5 Search for H/A with $\tau^+\tau^-$ final states

In Sec.3.1.4 we study the impact of the $H/A \rightarrow \tau^+\tau^-$ channel on the parameter space of interest using the LHC-8 data and find that regions with large $\tan\beta$ (>20) and M_A up to 600 GeV are already excluded. In this section, we discuss the sensitivity of the 14 TeV run of LHC to probe the remaining allowed region of parameter space via the $\tau^+\tau^-$ channel. In order to perform a detailed

signal-background analysis, we follow the ATLAS simulation with LHC-8 data [54]. We assume that H/A are produced via the b-quark associated production process and decays to $\tau^+\tau^-$. The ATLAS analysis [54] have shown that for M_A between 300 and 600 GeV, the final state with one leptonically decaying τ (τ_{lep}) and one hadronically decaying τ (τ_{had}) gives the best sensitivity (see Fig. 9(b) of Ref. [54]), and so in our analysis we consider the $H/A \rightarrow \tau_{\text{lep}}\tau_{\text{had}}$ signature only. We identify taus through their hadronic decays and demand that the candidate jet must lie within $|\eta| < 2.5$ with $p_T > 30$ GeV. The jet must contain one or three charged tracks with $|\eta_{\text{track}}| < 2.5$ and highest track $p_T > 3$ GeV. Moreover, in order to ensure proper charge track isolation, we also require that there are no other charged tracks with $p_T > 1$ GeV inside the candidate jet.

We select events with at least one lepton (electron/muon) with $p_T > 50$ GeV and an oppositely charged τ -hadron with $p_T > 50$ GeV. We further demand that events do not contain any additional electrons or muons, and the transverse momentum difference $\Delta p_T \equiv p_T(\tau_{\text{had}}) - p_T(\text{lepton})$ is greater than 50 GeV. Additionally, following Ref. [54], we also demand the sum of the azimuthal angles $\sum \Delta\phi \equiv \Delta\phi(\tau_{\text{had}}, \cancel{E}_T) + \Delta\phi(\tau_{\text{lep}}, \cancel{E}_T)$ is less than 3.3, and the hadronic and leptonic τ -decays satisfy $\Delta\phi(\tau_{\text{lep}}, \tau_{\text{had}}) > 2.4$. Besides, events with at least one b-tagged jet with $p_T > 50$ GeV are also selected. Finally, we demand that the reconstructed di-tau invariant mass ($m_{\tau\tau}$) is within $M_\Phi \pm 30$ GeV ($\Phi = H/A$). The dominant SM background processes that can mimic the signal are Z +jets, W +jets, QCD multi-jets and $t\bar{t}$. We analyze the most dominant SM backgrounds, namely Z +jets and $t\bar{t}$, while we check that QCD multi-jet contribution is negligibly small. In order to accommodate other subdominant backgrounds, we consider 50% enhancement of the total estimated background.

The signal events are generated using PYTHIA (version 6.4.28) [86] assuming H/A are produced via the b-quark associated production process. Here we concentrate on the region $200 < M_A < 600$ GeV and split the entire M_A region in steps of 25 GeV. For each event we then calculate the di-tau invariant mass using the “collinear approximation technique” with the assumption that the τ -lepton and all its decay products are collinear [106] and \cancel{E}_T in an event is entirely due to the neutrinos¹¹. After performing a bin-wise signal/background analysis, we thus obtain a 95% C.L. expected exclusion limit on the production cross sections for the signal events assuming $\text{BR}(H/A \rightarrow \tau^+\tau^-) = 100\%$. We calculate the production cross sections for all the points corresponding to our scanned data set, and then impose the estimated exclusion limits on the production cross sections for different values of M_A (or M_H). In Fig. 17(a), we display the distribution of the quantity $\sigma \times \text{Br}(H/A \rightarrow \tau^+\tau^-)$ when H/A are produced via the b-associated process. Similar to Fig. 9, we here also display the scanned data set with different $\tan\beta$ dependences. For example, the regions with $20 < \tan\beta < 50$, $10 < \tan\beta < 20$, $5 < \tan\beta < 10$ and $1 < \tan\beta < 5$ are shown in red (cross), pink (triangle), blue (circle) and green (square) respectively. The solid red and black lines indicate

¹¹Another technique often used by the experimental collaborations are the Missing Mass Calculator (MMC) method which allows a better reconstruction of the $\tau\tau$ invariant mass distribution [106]. In this paper, however, we restrict ourselves to the “collinear approximation technique”.

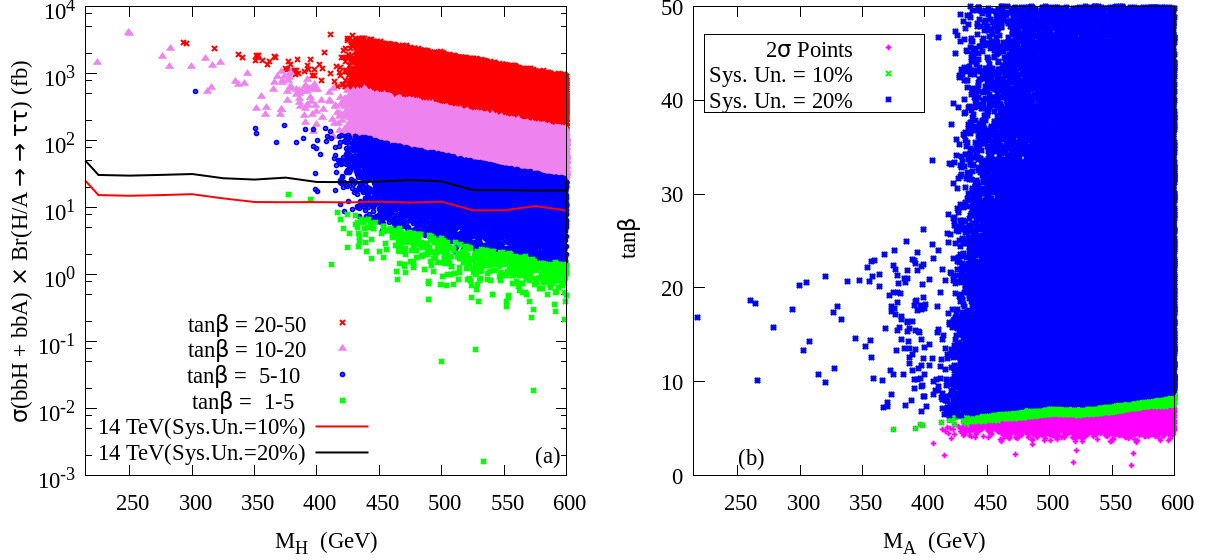


Figure 17: *Left: Scatter plot in $M_H - [\sigma \times \text{Br}(\Phi \rightarrow \tau^+\tau^-)]$ plane where $\Phi = H, A$ produced in association with b -quarks. The entire $\tan\beta$ region is splitted into different pieces, the regions with $20 < \tan\beta < 50$, $10 < \tan\beta < 20$, $5 < \tan\beta < 10$ and $1 < \tan\beta < 5$ are shown in red (cross), pink (triangle), blue (circle) and green (square) respectively. The solid red (black) line represents the expected upper limits on $\sigma \times \text{Br}(\Phi \rightarrow \tau^+\tau^-)$ at the HL-LHC with $\mathcal{L} = 3000 \text{ fb}^{-1}$. Right: Sensitivity of $H/A \rightarrow \tau^+\tau^-$ final states in $M_A - \tan\beta$ plane. The magenta (plus) points are the 2σ allowed points corresponding to our scanned data set, while the blue (square) and green (cross) points are expected to be probed at HL-LHC considering 20% and 10% systematic uncertainties respectively.*

the expected sensitivity in the HL-LHC with 10% and 20% systematic uncertainties respectively.

We have already mentioned that in the MSSM, the production cross sections and branching ratios of H and/or A crucially depend on two important parameters M_A and $\tan\beta$. Thus the expected sensitivity of the 14 TeV LHC on the H/A production cross sections can be translated in the $M_A - \tan\beta$ plane. In Fig. 17(b) we display such possibility where the magenta (plus) points denote our scanned data set while the blue (squared) and green (crossed) points represent the regions of parameter space in the $M_A - \tan\beta$ plane which can be probed at the high luminosity run of LHC with 3000 fb^{-1} of data assuming 20% and 10% systematic uncertainties respectively.

Thus, combining the existing 8 TeV direct search bounds (see Fig.9) and the estimated HL-LHC bounds, one can infer that the regions with $\tan\beta > 20$ are already excluded by LHC-8 data while the regions with $\tan\beta$ down to 8 with any values of M_A can be probed at the HL-LHC.

5 Conclusion

A scalar particle with mass close to 125 GeV has been discovered at the LHC. Measurements of spin-parity and various couplings seem to agree with the SM expectations. In the minimal extension of SM, namely MSSM, one can identify the observed 125 GeV Higgs boson as the lightest Higgs boson among the five MSSM Higgses h , H , A and H^\pm . In the MSSM, the couplings of h with the SM gauge bosons (W/Z) are proportional to $\sin(\beta - \alpha)$ where $\tan\beta$ is the ratio of vevs of two Higgs doublets while α is the Higgs mixing angle. Precise measurements of various couplings of the observed Higgs boson with W/Z bosons by the ATLAS and CMS collaborations imply $\sin(\beta - \alpha) \sim 1$. At the tree level, the Higgs mixing angle can be derived using pseudoscalar Higgs mass parameter M_A and $\tan\beta$, however if we include radiative corrections, α becomes a non-trivial function of various SUSY parameters. The ATLAS and CMS collaborations have also searched for the heavy Higgs bosons (H , A , H^\pm), however absence of any signal puts strong bounds on the masses/branchings of these heavy Higgses. One can easily satisfy the current LHC data by taking $\alpha \rightarrow 0$, and $\beta \rightarrow \pi/2$ with $M_A \gg M_Z$, which is generally known as the decoupling limit of MSSM. In this limit, the lightest MSSM Higgs boson behaves exactly like SM Higgs and masses of other Higgs bosons (H , A , H^\pm) are pushed well above LHC reach. In this paper we study the possibility of having light additional MSSM Higgs bosons, preferably below 600 GeV, with moderate Higgs mixing angle α , being consistent with the SM Higgs data and also direct search limits on the MSSM heavy Higgses.

We restrict ourselves to the 19 dimensional pMSSM framework and scan the parameters that are relevant for the MSSM Higgs sector. We perform a global fit analysis using most updated data (till December 2014) from the LHC and Tevatron experiments and also consider the flavor physics constraints. The region with $M_A \leq 350$ GeV and $\tan\beta \geq 25$ are excluded by the $\text{Br}(B_s \rightarrow \mu^+\mu^-)$ while $M_A \leq 350$ GeV with $\tan\beta \leq 8$ is not favoured by the $\text{Br}(b \rightarrow s\gamma)$ constraint. The regions with large M_A value (> 400 GeV) are not much constrained by the data. An interesting point to note that regions with $200 < M_A < 400$ can have moderate values of the Higgs mixing angle $\alpha = 0.2$, while for relatively large values of M_A , α can be as large as ~ 0.8 with small $\tan\beta$. Thus, one is not always forced to be in the decoupling limit to comply with the LHC data and light additional Higgses (M_A) are still allowed by the current data. Moreover, 10 - 20% deviations from the SM expectations are also observed for various Higgs signal strength variables.

We next study the impact of current bounds on the MSSM heavy Higgs boson (H , A and H^\pm) masses and couplings from the direct search at the LHC. We analyze the following decay modes of the MSSM heavy Higgses: $H \rightarrow \gamma\gamma$, $H \rightarrow WW$, $H \rightarrow hh \rightarrow b\bar{b}b\bar{b}$, $H \rightarrow hh \rightarrow b\bar{b}\gamma\gamma$, $H/A \rightarrow \tau^+\tau^-$, $A \rightarrow Zh$, $H^\pm \rightarrow \tau^\pm\nu$ and $H^\pm \rightarrow t\bar{b}$. As we have already mentioned, most of the regions of parameter space satisfy the alignment limit ($\beta - \alpha \sim \pi/2$), the 7+8 TeV LHC data on $H \rightarrow WW$ channel is not sensitive enough to constrain the parameter space of our interest. Except $H/A \rightarrow \tau^+\tau^-$, LHC bounds on the production cross section times branching ratios for other decay modes of H , A and

H^\pm are also one/two orders of magnitude larger compared to the MSSM expectations. The 7+8 TeV LHC data on MSSM heavy Higgs boson decay $\Phi(= H/A) \rightarrow \tau^+\tau^-$ put the most stringent bound on our parameter space. The entire region with $\tan\beta > 20$ is excluded when the heavy Higgses $\Phi = H/A$ are produced via $b\bar{b}\Phi$ process. The reason being large $\tan\beta$ (typically > 20) implies large $\text{Br}(H/A \rightarrow \tau^+\tau^-)$, typically $\sim 10\%$, and large cross section for associated production of H/A with bottom quarks, and thus stronger constraint on the quantity $\sigma \times Br$.

We also study the prospect of probing the allowed parameter space, mostly low $\tan\beta$ region, at the high luminosity run of LHC (HL-LHC). We impose the ATLAS and CMS preliminary results on $H \rightarrow ZZ$ and $A \rightarrow Zh$ at the HL-LHC. The impact of the future limits from the $H \rightarrow ZZ$ and $A \rightarrow Zh$ channels on the allowed parameter space are found to be marginal at $\mathcal{L} = 3000 \text{ fb}^{-1}$. Searches via $H \rightarrow hh$ at the HL-LHC can only probe a small part of the parameter space with low $\tan\beta$. Among several other possible decay modes, $H \rightarrow t\bar{t}$ dominates in the low $\tan\beta$ region for $M_H > 350 \text{ GeV}$. We perform a dedicated signal-background analysis on the $H \rightarrow t\bar{t}$ channel by choosing few representative MSSM benchmark points, and find that the signal to background ratio is very small. A more detailed analysis is required, for example one can use the jet substructure technique, spin correlation technique to achieve better sensitivity in this channel. We find that so far the combined 7+8 TeV LHC data on the $H/A \rightarrow \tau^+\tau^-$ channel has the best sensitivity to place constraints on the MSSM parameter space of interest. Thus, one may expect to find stronger constraints on the MSSM parameter space from the $\tau^+\tau^-$ mode at the HL-LHC. We study this possibility and find that combining the existing 8 TeV direct search bounds and the estimated HL-LHC bounds, one can infer that the regions with $\tan\beta > 20$ are already excluded by LHC-8 data while the regions with $\tan\beta$ down to 8 with low to moderate values of M_A can be probed at the HL-LHC. Below $\tan\beta < 8$, searches via $H \rightarrow hh$ at the HL-LHC can be very important to probe the parameter space.

In summary, we find that regions with low to moderate values of $\tan\beta$ with light additional Higgses (mass $\leq 600 \text{ GeV}$) remain unconstrained by the current data. Even the high luminosity run of LHC may not have enough sensitivity to probe the entire low $\tan\beta$ region of parameter space. However, the proposed e^+e^- international linear collider (ILC) will be an ideal machine to study this scenario. With the expected accuracies in the determination of various partial decay widths of the Higgs boson and also the possibility of producing some of the heavy MSSM Higgses directly, one might be able to probe the remaining region of the allowed parameter space with $\sqrt{s} = 1000 \text{ GeV}$ with higher luminosities at the ILC.

Acknowledgements:

We acknowledge Shankha Banerjee for useful discussions regarding global fits. Work of B. Bhattacharjee is supported by Department of Science and Technology, Government of INDIA under the Grant Agreement numbers IFA13-PH-75 (INSPIRE Faculty Award). A. Chakraborty would like to thank the Department

of Atomic Energy, Government of India for financial support. The work of A. Choudhury was partially supported by funding available from the Department of Atomic Energy, Government of India, for the Regional Centre for Accelerator-based Particle Physics (RECAPP), Harish-Chandra Research Institute.

References

- [1] G. Aad *et al.* ATLAS Collaboration, Phys. Lett. B **716**, 1 (2012) [[arXiv:1207.7214](#)].
- [2] S. Chatrchyan *et al.* CMS Collaboration, Phys. Lett. B **716**, 30 (2012) [[arXiv:1207.7235](#)].
- [3] T. Aaltonen *et al.* [CDF and D0 Collaborations], Phys. Rev. D **88**, no. 5, 052014 (2013) [[arXiv:1303.6346](#)].
- [4] G. Aad *et al.* [ATLAS Collaboration], Phys. Lett. B **738**, 68 (2014) [[arXiv:1406.7663](#)].
- [5] V. Khachatryan *et al.* [CMS Collaboration], [[arXiv:1410.6679](#)].
- [6] G. Aad *et al.* [ATLAS Collaboration], Phys. Rev. D **90**, no. 11, 112015 (2014) [[arXiv:1408.7084](#)].
- [7] V. Khachatryan *et al.* [CMS Collaboration], Eur. Phys. J. C **74**, no. 10, 3076 (2014) [[arXiv:1407.0558](#)].
- [8] G. Aad *et al.* [ATLAS Collaboration], [[arXiv:1412.2641](#)].
- [9] S. Chatrchyan *et al.* [CMS Collaboration], JHEP **1401**, 096 (2014) [[arXiv:1312.1129](#)].
- [10] G. Aad *et al.* [ATLAS Collaboration], Phys. Rev. D **91**, no. 1, 012006 (2015) [[arXiv:1408.5191](#)].
- [11] S. Chatrchyan *et al.* [CMS Collaboration], Phys. Rev. D **89**, no. 9, 092007 (2014) [[arXiv:1312.5353](#)].
- [12] G. Aad *et al.* [ATLAS Collaboration], JHEP **1501**, 069 (2015) [[arXiv:1409.6212](#)].
- [13] S. Chatrchyan *et al.* [CMS Collaboration], Phys. Rev. D **89**, no. 1, 012003 (2014) [[arXiv:1310.3687](#)].
- [14] The ATLAS collaboration, ATLAS-CONF-2014-061, ATLAS-COM-CONF-2014-080 [<https://cds.cern.ch/record/1954724>].
- [15] S. Chatrchyan *et al.* [CMS Collaboration], JHEP **1405**, 104 (2014) [[arXiv:1401.5041](#)].
- [16] G. Aad *et al.* [ATLAS Collaboration], Phys. Rev. D **90**, no. 5, 052004 (2014) [[arXiv:1406.3827](#)].
- [17] V. Khachatryan *et al.* [CMS Collaboration], [[arXiv:1412.8662](#)].
- [18] For reviews on Supersymmetry, see, J. Wess and J. Bagger, *Supersymmetry and Supergravity*, 2nd ed. (Princeton University Press, Princeton, 1991); M. Drees, P. Roy and R. M. Godbole, *Theory and Phenomenology of Sparticles*, (World Scientific, Singapore, 2005); H. E. Haber and G. Kane, Phys. Rep. **117**, 75 (1985); H. P. Nilles, Phys. Rep. **110**, 1 (1984).
- [19] S. P. Martin, [[arXiv:hep-ph/9709356](#)].
- [20] A. Djouadi, Phys. Rept. **459**, 1 (2008) [[arXiv:hep-ph/0503173](#)].
- [21] [CMS Public SUSY summary](#)

- [22] [ATLAS Public SUSY summary](#)
- [23] J. Ellis and T. You, JHEP **1206**, 140 (2012) [[arXiv:1204.0464](#)].
- [24] M. Klute, R. Lafaye, T. Plehn, M. Rauch and D. Zerwas, Phys. Rev. Lett. **109**, 101801 (2012) [[arXiv:1205.2699](#)].
- [25] J. Ellis and T. You, JHEP **1209**, 123 (2012) [[arXiv:1207.1693](#)].
- [26] T. Plehn and M. Rauch, Europhys. Lett. **100**, 11002 (2012) [[arXiv:1207.6108](#)].
- [27] G. Cacciapaglia, A. Deandrea, G. D. La Rochelle and J. B. Flament, JHEP **1303**, 029 (2013) [[arXiv:1210.8120](#)].
- [28] T. Corbett, O. J. P. Eboli, J. Gonzalez-Fraile and M. C. Gonzalez-Garcia, Phys. Rev. D **87**, 015022 (2013) [[arXiv:1211.4580](#)].
- [29] G. Belanger, B. Dumont, U. Ellwanger, J. F. Gunion and S. Kraml, JHEP **1302**, 053 (2013) [[arXiv:1212.5244](#)].
- [30] K. Cheung, J. S. Lee and P. Y. Tseng, JHEP **1305**, 134 (2013) [[arXiv:1302.3794](#)].
- [31] P. P. Giardino, K. Kannike, I. Masina, M. Raidal and A. Strumia, JHEP **1405**, 046 (2014) [[arXiv:1303.3570](#)].
- [32] J. Ellis and T. You, JHEP **1306**, 103 (2013) [[arXiv:1303.3879](#)].
- [33] A. Djouadi and G. Moreau, Eur. Phys. J. C **73**, no. 9, 2512 (2013) [[arXiv:1303.6591](#)].
- [34] K. Cheung, J. S. Lee, E. Senaha and P. Y. Tseng, JHEP **1406**, 149 (2014) [[arXiv:1403.4775](#)].
- [35] J. de Blas, M. Ciuchini, E. Franco, D. Ghosh, S. Mishima, M. Pierini, L. Reina and L. Silvestrini, [[arXiv:1410.4204](#)].
- [36] K. Cheung, J. S. Lee and P. Y. Tseng, [[arXiv:1501.03552](#)].
- [37] M. Endo, T. Moroi and M. M. Nojiri, [[arXiv:1502.03959](#)].
- [38] K. J. de Vries, E. A. Bagnaschi, O. Buchmueller, R. Cavanaugh, M. Citron, A. De Roeck, M. J. Dolan and J. R. Ellis *et al.*, [[arXiv:1504.03260](#)].
- [39] K. Cheung, J. S. Lee and P. Y. Tseng, JHEP **1401**, 085 (2014) [[arXiv:1310.3937](#)].
- [40] G. Belanger, B. Dumont, U. Ellwanger, J. F. Gunion and S. Kraml, Phys. Rev. D **88**, 075008 (2013) [[arXiv:1306.2941](#)].
- [41] A. Celis, V. Ilisie and A. Pich, JHEP **1307**, 053 (2013) [[arXiv:1302.4022](#)].
- [42] W. Altmannshofer, S. Gori and G. D. Kribs, Phys. Rev. D **86**, 115009 (2012) [[arXiv:1210.2465](#) [hep-ph]].
- [43] Y. Bai, V. Barger, L. L. Everett and G. Shaughnessy, Phys. Rev. D **87**, 115013 (2013) [[arXiv:1210.4922](#)].
- [44] S. Chang, S. K. Kang, J. P. Lee, K. Y. Lee, S. C. Park and J. Song, JHEP **1305**, 075 (2013) [[arXiv:1210.3439](#)].

- [45] H. S. Cheon and S. K. Kang, JHEP **1309**, 085 (2013) [[arXiv:1207.1083](#)].
- [46] U. Ellwanger and C. Hugonie, JHEP **1408**, 046 (2014) [[arXiv:1405.6647](#)].
- [47] D. Carmi, A. Falkowski, E. Kuflik and T. Volansky, JHEP **1207**, 136 (2012) [[arXiv:1202.3144](#)].
- [48] S. Banerjee, S. Mukhopadhyay and B. Mukhopadhyaya, JHEP **1210**, 062 (2012) [[arXiv:1207.3588](#)].
- [49] W. F. Chang, W. P. Pan and F. Xu, Phys. Rev. D **88**, no. 3, 033004 (2013) [[arXiv:1303.7035](#)].
- [50] J. Ellis, V. Sanz and T. You, [[arXiv:1410.7703](#)].
- [51] J. Ellis, V. Sanz and T. You, JHEP **1407**, 036 (2014) [[arXiv:1404.3667](#)].
- [52] S. Banerjee, S. Mukhopadhyay and B. Mukhopadhyaya, Phys. Rev. D **89**, no. 5, 053010 (2014) [[arXiv:1308.4860](#)].
- [53] J. R. Espinosa, C. Grojean, V. Sanz and M. Trott, JHEP **1212**, 077 (2012) [[arXiv:1207.7355](#)].
- [54] G. Aad *et al.* [ATLAS Collaboration], JHEP **1411**, 056 (2014) [[arXiv:1409.6064](#)].
- [55] V. Khachatryan *et al.* [CMS Collaboration], JHEP **1410**, 160 (2014) [[arXiv:1408.3316](#)].
- [56] CMS Collaboration, CMS-PAS-HIG-14-006 [<http://cds.cern.ch/record/1304533>].
- [57] CMS Collaboration, CMS-PAS-HIG-13-032 [<http://cds.cern.ch/record/1697512>].
- [58] CMS Collaboration, CMS-PAS-HIG-14-013 [<http://cds.cern.ch/record/1748425>].
- [59] CMS Collaboration, CMS-PAS-HIG-13-027 [<http://cds.cern.ch/record/1743804>].
- [60] G. Aad *et al.* [ATLAS Collaboration], Phys. Lett. B **744**, 163 (2015) [[arXiv:1502.04478](#)].
- [61] CMS Collaboration, CMS-PAS-HIG-14-011 [<http://cds.cern.ch/record/1969698>].
- [62] G. Aad *et al.* [ATLAS Collaboration], JHEP **1503**, 088 (2015) [[arXiv:1412.6663](#)].
- [63] CMS Collaboration, CMS-PAS-HIG-14-020 [<http://cds.cern.ch/record/1950346>].
- [64] G. Aad *et al.* [ATLAS Collaboration], Eur. Phys. J. C **73**, no. 6, 2465 (2013) [[arXiv:1302.3694](#)].
- [65] CMS Collaboration, CMS-PAS-HIG-13-035 [<http://cds.cern.ch/record/1728343>].
- [66] CMS Collaboration, CMS-PAS-HIG-13-026 [<http://cds.cern.ch/record/1755203>].
- [67] Y. Amhis *et al.* [Heavy Flavor Averaging Group (HFAG) Collaboration], [[arXiv:1412.7515](#)].
- [68] T. R. Junk and A. Juste, International Journal of Modern Physics A Vol. 30 (2015) 1541006 [[arXiv:1409.5043](#)].
- [69] Moriond 2014 updates: <http://moriond.in2p3.fr/QCD/2014/SundayMorning/DeFilippis.pdf>

- [70] G. Degrossi, S. Heinemeyer, W. Hollik, P. Slavich and G. Weiglein, Eur. Phys. J. C **28**, 133 (2003) [[arXiv:hep-ph/0212020](#)]; B. C. Allanach, A. Djouadi, J. L. Kneur, W. Porod and P. Slavich, JHEP **09**, 044 (2004) [[arXiv:hep-ph/0406166](#)]; S. P. Martin, Phys. Rev. D **75**, 055005 (2007) [[arXiv:hep-ph/0701051](#)]; R. V. Harlander, P. Kant, L. Mihaila and M. Steinhauser, Phys. Rev. Lett **100** 191602 (2008) [[arXiv:0803.0672](#)], Erratum: Phys. Rev. Lett **101** 039901 (2008); S. Heinemeyer, O. Stal and G. Weiglein, Phys. Lett. B **710**, 201 (2012) [[arXiv:1112.3026](#)]; A. Arbey, M. Battaglia, A. Djouadi and F. Mahmoudi, [[arXiv:1207.1348](#)].
- [71] A. Djouadi, J. L. Kneur and G. Moultaka, Comput. Phys. Commun. **176**, 426 (2007) [[arXiv:hep-ph/0211331](#)].
- [72] F. Mahmoudi, Comput. Phys. Commun. **178**, 745 (2008) [[arXiv:0710.2067](#)]; Comput. Phys. Commun. **180**, 1579 (2009) [[arXiv:0808.3144](#)]; Comput. Phys. Commun. **180**, 1718 (2009).
- [73] A. Djouadi, J. Kalinowski and M. Spira, Comput. Phys. Commun. **108**, 56 (1998) [[arXiv:hep-ph/9704448](#)].
- [74] LHC Higgs Cross-section Working Group: <https://twiki.cern.ch/twiki/bin/view/LHCPhysics/CrossSections>.
- [75] S. Eidelman *et al.* [Particle Data Group Collaboration], Phys. Lett. B **592**, 1 (2004).
- [76] K. Kowalska, L. Roszkowski, E. M. Sessolo and A. J. Williams, JHEP **1506**, 020 (2015) [[arXiv:1503.08219](#) [hep-ph]].
- [77] J. F. Gunion and H. E. Haber, Phys. Rev. D **67**, 075019 (2003) [[arXiv:hep-ph/0207010](#)].
- [78] A. Delgado, G. Nardini and M. Quiros, JHEP **1307**, 054 (2013) [[arXiv:1303.0800](#)].
- [79] N. Craig, J. Galloway and S. Thomas, [[arXiv:1305.2424](#)].
- [80] M. Carena, I. Low, N. R. Shah and C. E. M. Wagner, JHEP **1404**, 015 (2014) [[arXiv:1310.2248](#)].
- [81] M. Carena, D. Garcia, U. Nierste and C. E. M. Wagner, Nucl. Phys. B **577**, 88 (2000) [hep-ph/9912516].
- [82] L. J. Hall, R. Rattazzi and U. Sarid, Phys. Rev. D **50**, 7048 (1994) [hep-ph/9306309, hep-ph/9306309].
- [83] J. Guasch, P. Hafliger and M. Spira, Phys. Rev. D **68**, 115001 (2003) [hep-ph/0305101].
- [84] S. Dawson, C. B. Jackson and P. Jaiswal, Phys. Rev. D **83**, 115007 (2011) [[arXiv:1104.1631](#) [hep-ph]].
- [85] R. V. Harlander, S. Liebler and H. Mantler, Comput. Phys. Commun. **184**, 1605 (2013) [[arXiv:1212.3249](#)]; R. V. Harlander and W. B. Kilgore, Phys. Rev. Lett. **88**, 201801 (2002) [[arXiv:hep-ph/0201206](#)]; Phys. Rev. D **68**, 013001 (2003) [[arXiv:hep-ph/0304035](#)]; U. Aglietti, R. Bonciani, G. Degrossi and A. Vicini, Phys. Lett. B **595**, 432 (2004) [[arXiv:hep-ph/0404071](#)]; G. Degrossi and P. Slavich, JHEP **1011**, 044 (2010) [[arXiv:1007.3465](#)]; G. Degrossi, S. Di Vita and P. Slavich, JHEP **1108**, 128 (2011) [[arXiv:1107.0914](#)]; R. Harlander and P. Kant, JHEP **0512**, 015 (2005) [[arXiv:hep-ph/0509189](#)].
- [86] T. Sjostrand, S. Mrenna and P. Z. Skands, JHEP **0605**, 026 (2006) [[arXiv:hep-ph/0603175](#)].

- [87] The ATLAS collaboration, ATLAS-CONF-2014-005, ATLAS-COM-CONF-2014-007 [<https://cds.cern.ch/record/1666518>].
- [88] [LEP Higgs Working Group for Higgs boson searches and ALEPH and DELPHI and L3 and OPAL Collaborations], [[arXiv:hep-ex/0107031](https://arxiv.org/abs/hep-ex/0107031)].
- [89] W. Altmannshofer, M. Carena, N. R. Shah and F. Yu, JHEP **1301**, 160 (2013) [[arXiv:1211.1976](https://arxiv.org/abs/1211.1976)].
- [90] M. Carena, S. Heinemeyer, O. Stl, C. E. M. Wagner and G. Weiglein, Eur. Phys. J. C **73**, no. 9, 2552 (2013) [[arXiv:1302.7033](https://arxiv.org/abs/1302.7033)].
- [91] M. Carena, H. E. Haber, I. Low, N. R. Shah and C. E. M. Wagner, Phys. Rev. D **91**, no. 3, 035003 (2015) [[arXiv:1410.4969](https://arxiv.org/abs/1410.4969)].
- [92] E. Arganda, J. L. Diaz-Cruz and A. Szykman, Eur. Phys. J. C **73**, no. 4, 2384 (2013) [[arXiv:1211.0163](https://arxiv.org/abs/1211.0163)]; Phys. Lett. B **722**, 100 (2013) [[arXiv:1301.0708](https://arxiv.org/abs/1301.0708)].
- [93] P. S. B. Dev and A. Pilaftsis, JHEP **1412**, 024 (2014) [[arXiv:1408.3405](https://arxiv.org/abs/1408.3405)].
- [94] ATLAS collaboration, ATL-PHYS-PUB-2013-016 [<https://cds.cern.ch/record/1611190/>].
- [95] CMS Collaboration, CMS-PAS-FTR-13-024 [<http://cds.cern.ch/record/1607086>].
- [96] B. Bhattacharjee and A. Choudhury, Phys. Rev. D **91**, 073015 (2015) [[arXiv:1407.6866](https://arxiv.org/abs/1407.6866)].
- [97] C. Han, X. Ji, L. Wu, P. Wu and J. M. Yang, JHEP **1404**, 003 (2014) [[arXiv:1307.3790](https://arxiv.org/abs/1307.3790)].
- [98] Higgs cross sections for European Strategy studies in 2012, <https://twiki.cern.ch/twiki/bin/view/LHCPhysics/HiggsEuropeanStrategy2012>, M. Spira, [<http://tiger.web.psi.ch/hpair/>] (2012).
- [99] D. E. Ferreira de Lima, A. Papaefstathiou and M. Spannowsky, JHEP **1408**, 030 (2014) [[arXiv:hep-ph/1404.7139](https://arxiv.org/abs/hep-ph/1404.7139)].
- [100] U. Baur, T. Plehn and D. L. Rainwater, Phys. Rev. D **69**, 053004 (2004) [[arXiv:hep-ph/0310056](https://arxiv.org/abs/hep-ph/0310056)].
- [101] ATLAS Collaboration, ATL-PHYS-PUB-2012-004 [<http://cds.cern.ch/record/1484890>].
- [102] ATLAS Collaboration, ATLAS-CONF-2012-043 [<https://cds.cern.ch/record/1435197>].
- [103] G. Aad *et al.* [ATLAS Collaboration], JHEP **1409**, 176 (2014) [[arXiv:1405.7875](https://arxiv.org/abs/1405.7875)].
- [104] <https://twiki.cern.ch/twiki/bin/view/LHCPhysics/TtbarNNLO>
- [105] A. Djouadi, L. Maiani, A. Polosa, J. Quevillon and V. Riquer, [[arXiv:1502.05653](https://arxiv.org/abs/1502.05653)].
- [106] A. Elagin, P. Murat, A. Pranko and A. Safonov, Nucl. Instrum. Meth. A **654**, 481 (2011) [[arXiv:1012.4686](https://arxiv.org/abs/1012.4686)].